The Canadian Mineralogist
Vol. 60, pp. 957-987 (2022)
DOI: 10.3749/canmin.2100032

THE MAGMATIC–HYDROTHERMAL TRANSITION IN LITHIUM PEGMATITES: PETROGRAPHIC AND GEOCHEMICAL CHARACTERISTICS OF PEGMATITES FROM THE KAMATIVI AREA, ZIMBABWE

RICHARD A. SHAW[§]

British Geological Survey, Environmental Science Centre, Nicker Hill, Keyworth, Nottingham NG12 5GG, UK

KATHRYN M. GOODENOUGH AND EIMEAR DEADY

British Geological Survey, The Lyell Centre, Research Avenue South, Edinburgh EH14 4AP, UK

PAUL NEX

University of the Witwatersrand, 1 Jan Smuts Avenue, Braamfontein 2000, Johannesburg, South Africa

BRIAN RUZVIDZO

Zimbabwe Lithium, 8 Park road, Suburbs, Bulawayo, Zimbabwe

JEREMY C. RUSHTON AND IAN MOUNTENEY

British Geological Survey, Environmental Science Centre, Nicker Hill, Keyworth, Nottingham NG12 5GG, UK

ABSTRACT

Lithium is a critical metal, vital for electrification of transport. Currently, around half the world's lithium is extracted from rare-metal pegmatites and understanding the genesis and evolution of these igneous rocks is therefore essential. This paper focuses on the pegmatites in the Kamativi region of Zimbabwe. A group of early pegmatites is distinguished from a late pegmatite suite which includes the *ca*. 1030 Ma Main Kamativi Pegmatite. Previously mined for tin, the mine tailings are now being investigated for lithium. Mineral-scale investigation of samples from the Main Kamativi Pegmatite has allowed recognition of a four-stage paragenesis: (1) an early magmatic assemblage dominated by quartz, alkali feldspar, spodumene ($LiAlSi_2O_6$) and montebrasite [$LiAl(PO_4)(OH, F)$]; (2) partial alteration by widespread albitization, associated with growth of cassiterite and columbite group minerals; (3) irregular development of a quartz, muscovite, columbite group mineral assemblage; and (4) widespread low-temperature fluid-induced alteration of earlier phases to cookeite, sericite, analcime, and apatite. Whole-rock geochemistry indicates that the late pegmatites are enriched in Li, Cs, Ta, Sn, and Rb but depleted in Nb, Zr, Ba, Sr, and the rare earth elements relative to early pegmatites and country rock granitoids. A combination of field relationships and published dating indicates that the granitoids, and probably the early pegmatites, were emplaced toward the end of the *ca*. 2000 Ma Magondi Orogeny, whereas the late pegmatites are almost 1000 million years younger. The late pegmatites thus cannot be genetically related to the granitoids and are instead likely to have formed by partial melting of metasedimentary source rocks. The drivers for this melting may be related to crustal thickening along the northern margin of the Kalahari Craton during the assembly of Rodinia.

Keywords: Lithium, tin, tantalum, pegmatite, Zimbabwe.

[§] *Corresponding author e-mail address*: rashaw@bgs.ac.uk

Introduction

As the world moves toward a low-carbon future, there is increasing demand for a range of raw materials used in electric vehicles and other green energy technologies. Lithium, used in batteries, is an example of a raw material for which demand is likely to rapidly increase (Pehlken *et al*. 2017). Around half of the world's lithium is currently extracted from evaporative brines, largely in South America, with the other half derived from rare-metal pegmatites in Australia, Zimbabwe, and other countries (USGS 2018). A specific family of rare-metal pegmatites, known as the LCT (Li-Cs-Ta) pegmatites (Černý & Ercit 2005), represent significant global resources of lithium, tin, tantalum, and caesium. However, there is still significant controversy over their genesis, and the geological controls on lithium mineralization are uncertain (Bradley *et al*. 2017). Many rare-metal pegmatites are characterized by complex zonation, which has been the subject of extensive investigation (London 2014). However, some economically important lithium pegmatites, for example those in the Tin-Spodumene Belt, USA (Swanson 2012); the Central Iberian Zone of Spain and Portugal (Roda-Robles *et al*. 2016); Mt. Cattlin, Australia (Sweetapple *et al*. 2019); Jiajika, China (Dai *et al*. 2019); and Goulamina, Mali (Wilde *et al*. 2021), lack the classic concentric internal zonation described by Cameron *et al*. (1949), Norton (1983), and London (2014). In recent years, there has been an increasing research focus on such pegmatites because of their importance for Li-Cs-Ta-Sn mineralization (Martins *et al*. 2011, 2012, London 2018, Dai *et al*. 2019, Ballouard *et al*. 2020, Barros *et al*. 2020, Simmons *et al*. 2020).

The classically accepted model for rare-metal pegmatites is that they represent the most highly fractionated melts produced from parental granitic plutons (Černý 1992, Černý *et al*. 2012b). A contrasting model, that rare-metal pegmatites are formed directly by low-degree partial melting of a fertile metasedimentary source, has existed for many years (Stewart 1978), but strong arguments have been put forward against this model (London 2005). In recent years, however, precise dating of pegmatites and granites has shown that some rare-metal pegmatites are notably younger than adjacent granitic magmatism (Goodenough *et al*. 2014, Zhang *et al*. 2016), and rare-metal pegmatites have been recognized in areas where there is no evidence of a parental granite (Shaw *et al*. 2016, Müller *et al*. 2017). Additionally, geochemical modeling demonstrates that, while a link can be demonstrated between some rare-metal pegmatites and their adjacent granite plutons (Roda-Robles *et al*. 2018, Garate-Olave *et al*. 2020), this is not always the case (Barros & Menuge 2016, Simmons *et al*. 2016, Fuchsloch *et al*. 2018, Villaros & Pichavant 2019). The weight of evidence thus suggests that both models have a place in understanding the genesis of rare-metal pegmatites. To improve exploration targeting for mineralization in pegmatites, it will be necessary to understand a range of issues, including the types of sources that are most likely to be prospective for rare-metal pegmatites, the most favorable geological settings, and the transport, emplacement, and evolution of magmas from which pegmatites are formed.

Zimbabwe is currently the world's fifth largest lithium producer (USGS 2018) and has substantial pegmatite lithium resources. Several important rare-metal pegmatites of Archaean to Proterozoic age occur within the Zimbabwe Craton (Melcher *et al*. 2017, Dittrich *et al*. 2019), typically intruded into greenstone belts (Von Knorring & Condliffe 1987). These include the Bikita pegmatite, which is actively mined and is the source of Zimbabwe's current lithium production. Exploration for lithium is also ongoing at the Arcadia pegmatite close to Harare and at Kamativi in northwestern Zimbabwe (Fig. 1). The latter is the subject of this paper.

The lithium-tin pegmatites of the Kamativi mine were mined for tin until the 1990s, and both the pegmatites and the previously crushed/milled mine tailings are now being investigated for lithium (Shaw *et al*. 2019). The tailings at Kamativi, which are currently being evaluated by Zimbabwe Lithium, comprise fine-grained (<1 mm) quartz, plagioclase, potassium feldspar, muscovite, and a range of lithium minerals, of which spodumene is the most abundant. The indicated resource estimate in the tailings at Kamativi currently stands at 26 million tonnes grading 0.6% Li_2O (Cronwright & Derbyshire 2018, Zimbabwe Lithium 2020). The mined intrusion is known as the Main Kamativi Pegmatite, but many other pegmatites also occur within the Archaean to Palaeoproterozoic metasedimentary rocks of the Dete-Kamativi inlier (Glynn *et al*. 2020). The Main Kamativi Pegmatite is well dated (U-Pb in coltan) at *ca*. 1030 Ma (Melcher *et al*. 2015, Glynn *et al*. 2017), placing it in the same broad time bracket as the extensive rare-metal pegmatites of the Kibaran Belt in Rwanda, Burundi, and the DRC (Melcher *et al*. 2017). However, it is much younger than nearby granitic plutons, which are dated (U-Pb in zircon) at *ca*. 2060–2020 Ma (Glynn *et al*. 2017). The Main Kamativi Pegmatite is thus an excellent case study of a pegmatite that appears to lack a parental granite. We present field, petrographic, mineralogical, and geochemical data to fully characterize the Main Kamativi Pegmatite and better understand its genesis and to

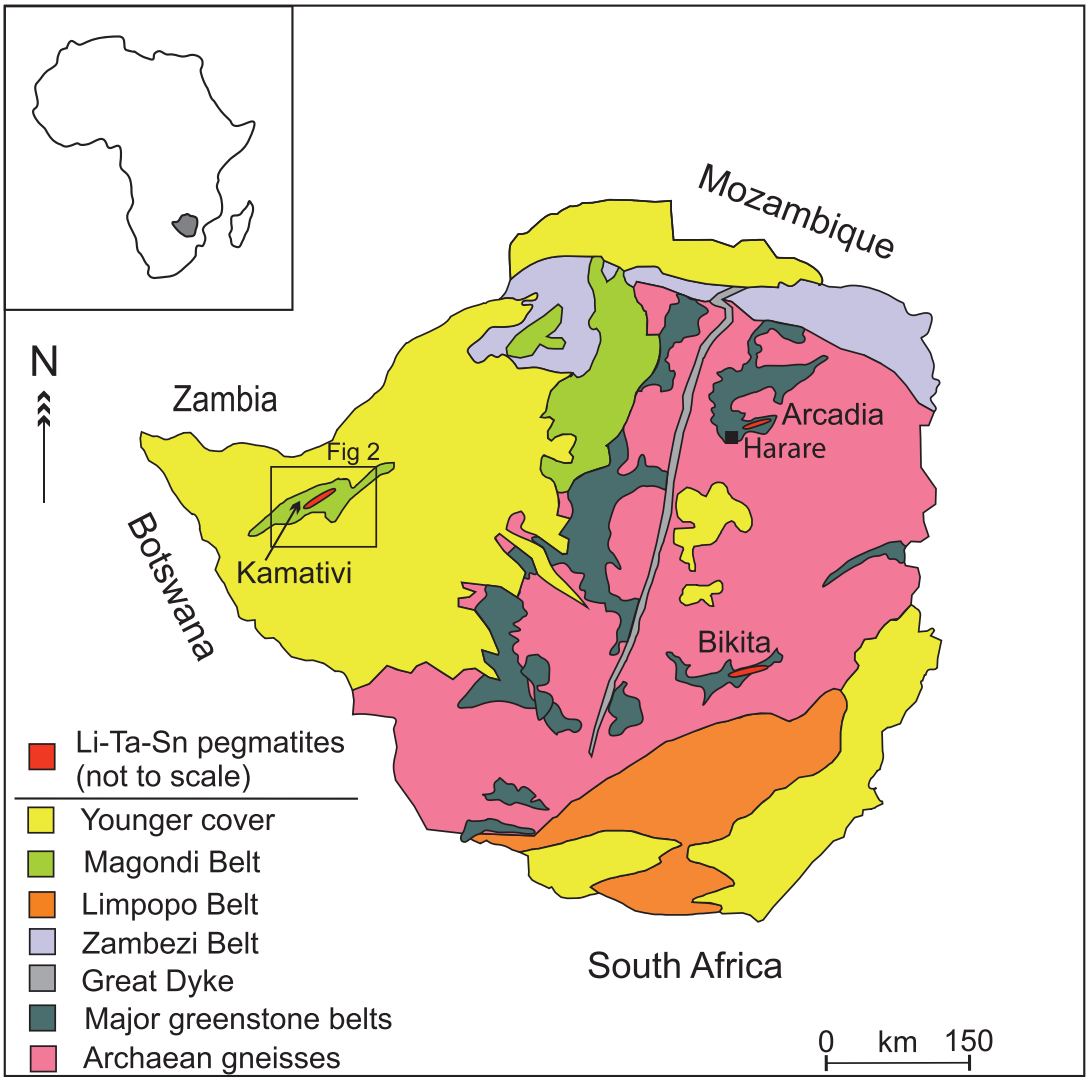

FIG. 1. Simplified geological map of Zimbabwe, after Markwitz *et al*. (2010) and Master *et al*. (2010).

investigate the mineral paragenesis of this globally important example of a potentially economic lithium pegmatite.

GEOLOGICAL SETTING

The Archaean craton of Zimbabwe has an extensive history of cratonic growth, extending from *ca*. 3570 to 2620 Ma (Horstwood *et al*. 1999). Greenstone belts, largely formed around 2700 Ma (Jelsma & Dirks 2002), make up around 20% of the craton (Fig. 1), and the craton is intruded by Neoarchaean post-tectonic granitoids (Rollinson & Whitehouse 2011). Rare-metal pegmatites, including that at Bikita, intruded into the greenstone belts at *ca*. 2600 Ma (Melcher *et al*. 2015), placing them in broad temporal association with the post-tectonic granitoid magmatism and the formation of orogenic gold deposits in the craton (Jelsma *et al*. 1996). The last major Archaean event in the Zimbabwe Craton was the emplacement of the Great Dyke, a 550 km-long layered intrusion, at *ca*. 2575 Ma (Oberthür *et al*. 2002). On the southern side of the craton is the Archaean Limpopo Belt, which underwent repeated phases of metamorphism during the Archaean and Palaeoproterozoic (Holzer *et al*. 1998). The northwestern margin of the craton is marked by

the Palaeoproterozoic Magondi Mobile Belt, which lies unconformably on Archaean gneiss of the Zimbabwe Craton (Fig. 1). The mobile belt contains a largely metasedimentary succession, the Magondi Supergroup, which was deposited around 2200–2100 Ma (Sawada *et al*. 2019), then metamorphosed and deformed at *ca*. 2000–1900 Ma (Master *et al*. 2010). It comprises three stratigraphic groups: the Deweras Group (formed in a terrestrial setting), the Lomagundi Group (marginal marine), and the Piriwiri Group (continental shelf to deep marine) (Master *et al*. 2010). The Magondi Mobile Belt is truncated by the Neoproterozoic (Pan-African) Zambezi Belt (Hargrove *et al*. 2003). Further northwest, in Zambia, Mesoproterozoic magmatism and sedimentation are recorded in the Choma-Kalomo Block (Glynn *et al*. 2017). The northern and southern parts of Zimbabwe are partly covered by younger sedimentary rocks.

The pegmatites of the Kamativi area occur within the Dete-Kamativi inlier of western Zimbabwe (Fig. 2). This is a broadly northeast-southwest trending belt of Precambrian metamorphic rocks, surrounded by Mesozoic Karoo sedimentary rocks and Cenozoic aeolian sands of the Kalahari Group (Lockett 1979). It comprises Archaean granodioritic orthogneisses (*ca*. 2700 Ma), Palaeoproterozoic granitoids (2080–2010 Ma), and a metasedimentary sequence which is divided into the Malaputese, Inyantue, Kamativi, and Tshontanda formations (Master *et al*. 2010, Glynn *et al*. 2020). The Malaputese and Inyantue formations are correlated with the Lomagundi and Deweras groups, whereas the Kamativi and Tshontanda formations correlate with the Piriwiri Group (Master *et al*. 2010). Detrital zircon dating suggests that all the metasedimentary formations were derived, at least in part, by erosion of an Archaean source (Glynn 2017, Glynn *et al*. 2020). These metasedimentary rocks have been strongly deformed and metamorphosed to amphibolite and granulite facies, and this deformation is generally considered to correlate with thrusting of these rocks onto the margin of the Zimbabwe Craton during the *ca*. 2060–1960 Ma Magondi Orogeny (Master *et al*. 2010, Glynn *et al*. 2017). The pegmatites in the Kamativi area are focused within metasedimentary rocks of the Kamativi and Tshontanda Formations, which comprise muscovite and biotite schists and psammites that typically contain garnet and tourmaline as accessory minerals (Lockett 1979).

The pegmatites of the Kamativi area were originally described by Rijks & van der Veen (1972). They noted the presence of two pegmatite groups: (1) tourmaline pegmatites, which are up to a few meters thick and have strike and dip parallel to the foliation in the metasedimentary host rocks, and (2) large (up to 30 m thick), shallowly dipping cassiterite pegmatites, emplaced as dome-like structures into the Precambrian metasedimentary rocks and clearly cross-cutting the fabrics in the host rocks. Steeply dipping tourmaline pegmatites were mined for mica at the Paolo Mine, southwest of Kamativi, and for tin at Kalinda, east of

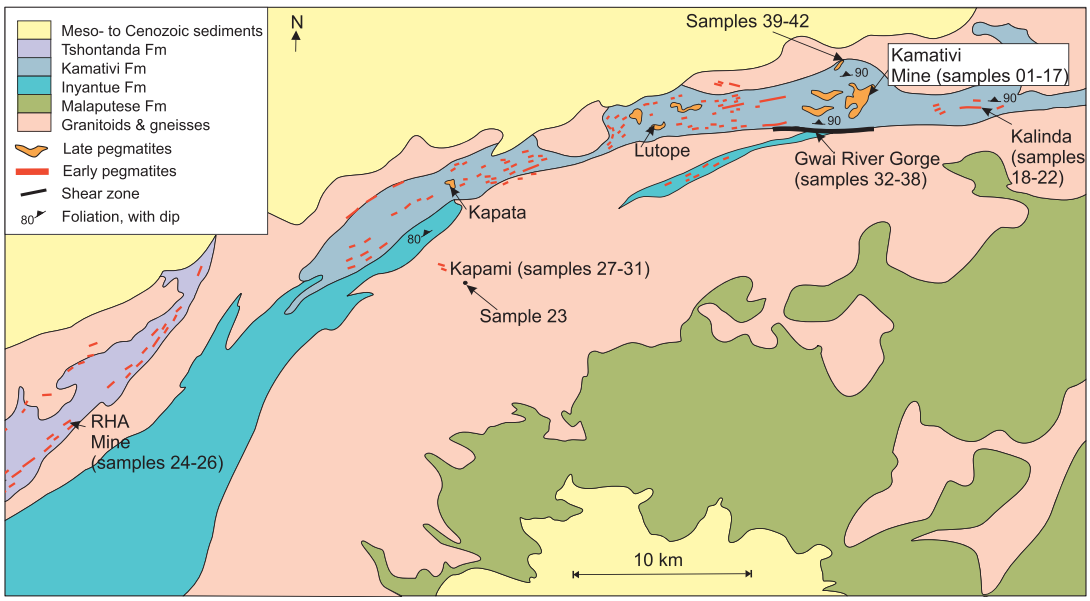

FIG. 2. Simplified geological map of the Dete-Kamativi area, after Lockett (1979), showing sample localities.

Kamativi (Lockett 1979). The shallowly dipping pegmatites were mined for tin in the Kamativi area from 1937 to 1994 (Kinnaird *et al*. 2016), and similar pegmatites were mined at Kapata and Lutope to the west of Kamativi (Lockett 1979) (Fig. 2). Much of this mining was artisanal to small-scale, with Kamativi being the only large-scale mine. At Kamativi, the cassiterite pegmatites were studied in both core and open pit and shown to have several branches or 'lobes' all dipping eastwards or westwards at around 10 to 20° (Rijks & van der Veen 1972). These pegmatites have muscovite-quartz border zones, up to 40 cm thick, and their cores contain coarse-grained alkali feldspar-quartz-spodumene assemblages together with finer-grained albite-quartz assemblages (Rijks & van der Veen 1972). Cassiterite, columbite group minerals (CGM), tourmaline, and beryl are all present in these shallowly dipping pegmatites.

The cassiterite pegmatites of the Kamativi area have been dated (U-Pb in coltan) at *ca*. 1030 Ma (Melcher *et al*. 2015, Glynn *et al*. 2017). This places them within the 940–1040 Ma age range of the Orange River Pegmatite Belt on the Namibia–South Africa border (Ballouard *et al*. 2020). Somewhat younger ages (*ca*. 930 Ma) have been obtained from pegmatites in the Choma-Kalomo Block in Zambia (Glynn *et al*. 2017). These dates correspond with a pulse of tin granitoid and pegmatite formation in the Kibaran and Karagwe-Ankole belts of Central Africa (Tack *et al*. 2010), although the two blocks are generally not considered to have been contiguous at that time (Johnson *et al*. 2005). The lithium-bearing cassiterite pegmatites of the Kamativi area can thus be considered part of a major Ta-Sn-W-Li metallogenetic belt which extends from Rwanda and Burundi, through the Democratic Republic of Congo, to Zambia, Zimbabwe, and Namibia (Melcher *et al*. 2015). Argon-Ar dating of biotite and muscovite from the metasedimentary rocks of the Dete-Kamativi inlier suggests a regional thermal event at *ca*. 1050–950 Ma (Glynn *et al*. 2017), which may be related to the pegmatite emplacement event. This thermal peak has not been linked to any specific deformation event that has previously been described in the inlier or in the Magondi Mobile Belt. It may be related to tectonism and post-collisional granitoids of similar age in the Irumide Belt of Zambia (De Waele *et al*. 2003, De Waele *et al*. 2006), although it is not certain whether the Irumide Belt extended into north-western Zimbabwe (Glynn *et al*. 2017).

Field Relationships

We carried out fieldwork in the Kamativi area in November 2018, and the information in this section is largely based on primary observations from that fieldwork, with some data from published literature. The focus of fieldwork was on the area around the Kamativi mine (Fig. 2), including artisanal workings at Kalinda and Kapami. A visit was also made to the Premier African Minerals RHA tungsten mine to the west of Kamativi. Due to difficulties with access, the pegmatites at Lutope were not visited.

The country rocks in the area around the Kamativi mine are steeply dipping pelitic to semi-pelitic schists of the Kamativi Formation. These have a strong foliation which generally dips steeply southwards and is axial planar to tight outcrop-scale folds. At some locations the pelitic schists appear migmatitic, with irregular granitic leucosomes (Lockett 1979). The Inyantue Formation, which outcrops to the south of the main belt of the Kamativi Formation, comprises largely garnetiferous schists and gneisses with some calcareous rocks, graphitic schists, and quartzites (Lockett 1979). These metasedimentary rocks are intruded by the Palaeoproterozoic granitoid plutons that make up much of the Dete-Kamativi inlier. These are coarse-grained biotite granites to granodiorites, locally containing tabular feldspars up to 2 cm in length. They typically carry a weak foliation, which across much of the area appears to have formed due to deformation while the melt was crystallizing. Biotite-rich country rock xenoliths up to 10 cm in size are locally common and elongated parallel to the foliation. Contacts between the granitoids and metasedimentary rocks are generally highly sheared and intrusive relationships are not always evident.

Two distinct types of granitic pegmatite are found in the Kamativi area: (1) vertical, or steeply dipping (*ca*. 80–90°), pegmatites that strike parallel to the foliation in the metasedimentary country rocks; and (2) shallowly dipping (*ca*. 10–20°) rare-metal pegmatites, and associated aplites, that cross-cut fabrics in the country rock. These two distinct types correspond to those described by Rijks & van der Veen (1972). Cross-cutting relationships are clear, with shallowly dipping pegmatites being demonstrably younger than the vertical pegmatites. From here on, steeply dipping, foliation parallel pegmatites will be termed 'early' and shallowly dipping, cross-cutting pegmatites will be termed 'late'.

Relationships between early and late pegmatites in the Kamativi area are particularly well-displayed in the Gwai River Gorge, to the south of the Kamativi mine (Fig. 2). Here country rocks that have been ascribed to the Inyantue Formation (Lockett 1979) are intensely deformed, with a strong, near-vertical, east–west striking foliation. Early pegmatites are white-weathering granitic pegmatites, up to 50 cm wide, which appear highly deformed and transposed into the

foliation. Contacts are sharp and generally parallel to the country rock, although locally very low-angle cross-cutting relationships can be seen, indicating that intrusion may have occurred during deformation. These pegmatites contain feldspar augen up to 2 cm in size in a strongly deformed quartzofeldspathic matrix (Fig. 3A). These features were originally described by Lockett (1979) as representing a 'transition' from pelitic schists to granitic gneisses. Late pegmatite and aplite intrusions at this locality are sharply bounded, up to 30 cm thick, and clearly cross-cut the foliation in the country rocks and the early pegmatites (Fig. 3A). The age of the deformation in the Gwai River Gorge is not known, but the intensity of deformation is indicative of a shear zone, most likely formed during the Magondi Orogeny. The lateral extent of this shear zone has not been mapped, although Lockett (1979) indicated that the southern margin of the Kamativi Formation in this area is highly sheared along much of its length.

Elsewhere in the field area, early pegmatites are typically between 1 and 5 m across and have sharp but locally irregular contacts with the country rock. They are typically parallel to the main foliation (Fig. 3B), but may locally cross-cut it at a low angle, and their margins may be foliated. Early pegmatites tend to be massive and unzoned, or may have a quartz core. They also lack graphic growth textures, and there is little evidence of unidirectional mineral growth. They largely comprise coarse-grained (up to 5 cm across) quartz and alkali feldspar, with books of gray-green mica and minor disseminated garnet and black tourmaline. Excellent examples of early pegmatites up to 20 cm thick were seen in core from the RHA Mine; these are foliation parallel and contain abundant black tourmaline crystals, particularly in the pegmatite core. The field relationships of the early pegmatites are generally consistent with emplacement toward the later stages of deformation in the host rocks, when deformation had become focused into discrete shear zones such as that in the Gwai River Gorge.

Late pegmatites in the Kamativi area are variable in size, ranging from tens of centimeters to tens of meters in thickness, and have sharp, yet highly irregular, contacts with their host rocks. The most remarkable example of a late pegmatite in the Kamativi area is the Main Kamativi Pegmatite, which is up to 30 m thick and extends laterally for hundreds of meters. This pegmatite is well-exposed in the large open pit formed by the old tin mine (Fig. 3C). It forms a broad domed sheet, with sharp contacts dipping away from the center of the dome at $<20°$, cross-cutting folds and foliation in the country rocks at a high angle. In the pit, a number of large rafts of country rock can be seen within the pegmatite (Fig. 3D), and past drilling and mining has shown that it splits into a series of lobes at depth (Rijks & van der Veen 1972). The country rock rafts appear undisturbed, with foliation parallel to the regional trend away from the pegmatite intrusion, suggesting relatively passive emplacement of the melts that formed the pegmatite.

Smaller-scale late pegmatites occur at Kapami (Fig. 2), where shallowly dipping pegmatite sheets (up to 30 cm thick) cut foliated granitoid rocks of the Dete-Kamativi inlier. The pegmatites clearly cut across the foliation in the granitoids, and contacts are sharp (Fig. 3E).

The Main Kamativi Pegmatite is characterized by largely unmineralized marginal zones up to *ca*. 50 cm thick, described as muscovite-quartz border zones by Rijks & van der Veen (1972). The core region of the Main Kamativi Pegmatite is the mineralized zone. It is not classically zoned, but does show some banding (Fig. 3F), which typically comprises alternating bands of finer-grained aplitic material up to a few cm thick and coarser-grained bands containing spodumene, alkali feldspar, and quartz. The bands are typically shallowly dipping and appear to be broadly parallel to the pegmatite margins. The late pegmatites also show a general lack of graphic growth textures, although unidirectional growth of tourmaline is seen in the pegmatites at Kapami. Another feature of the late pegmatites is the local development of irregularly shaped areas of cassiterite-bearing, mica-rich greisen, which appear to be most prevalent where late pegmatites are in contact with the country rock. Adjacent to the pegmatite, country rock schists typically show evidence of metasomatism at the contact, with growth of acicular amphibole and/or tourmaline.

Analytical Methods

The focus of this work was the pegmatites at Kamativi. This, and the logistical challenges encountered during fieldwork, which included severe fuel shortages, restricted access, and issues associated with the export of samples, dictated the number, type, and mass of samples collected. In total 42 bulk-rock samples of between 0.5 and 5 kg in weight were collected from across the Kamativi area, including pegmatites, country rocks, and granitoids. The authors are aware of the potential issues associated with sampling very coarse-grained rocks and made sure that samples comprised carefully selected rock fragments and drill core that were typical of the exposure being sampled. A polished thin section was prepared for each of the 42 samples. A sub-set of 18 samples that were considered to be representative of the granitoids, pegmatites, and aplites in the Kamativi area was

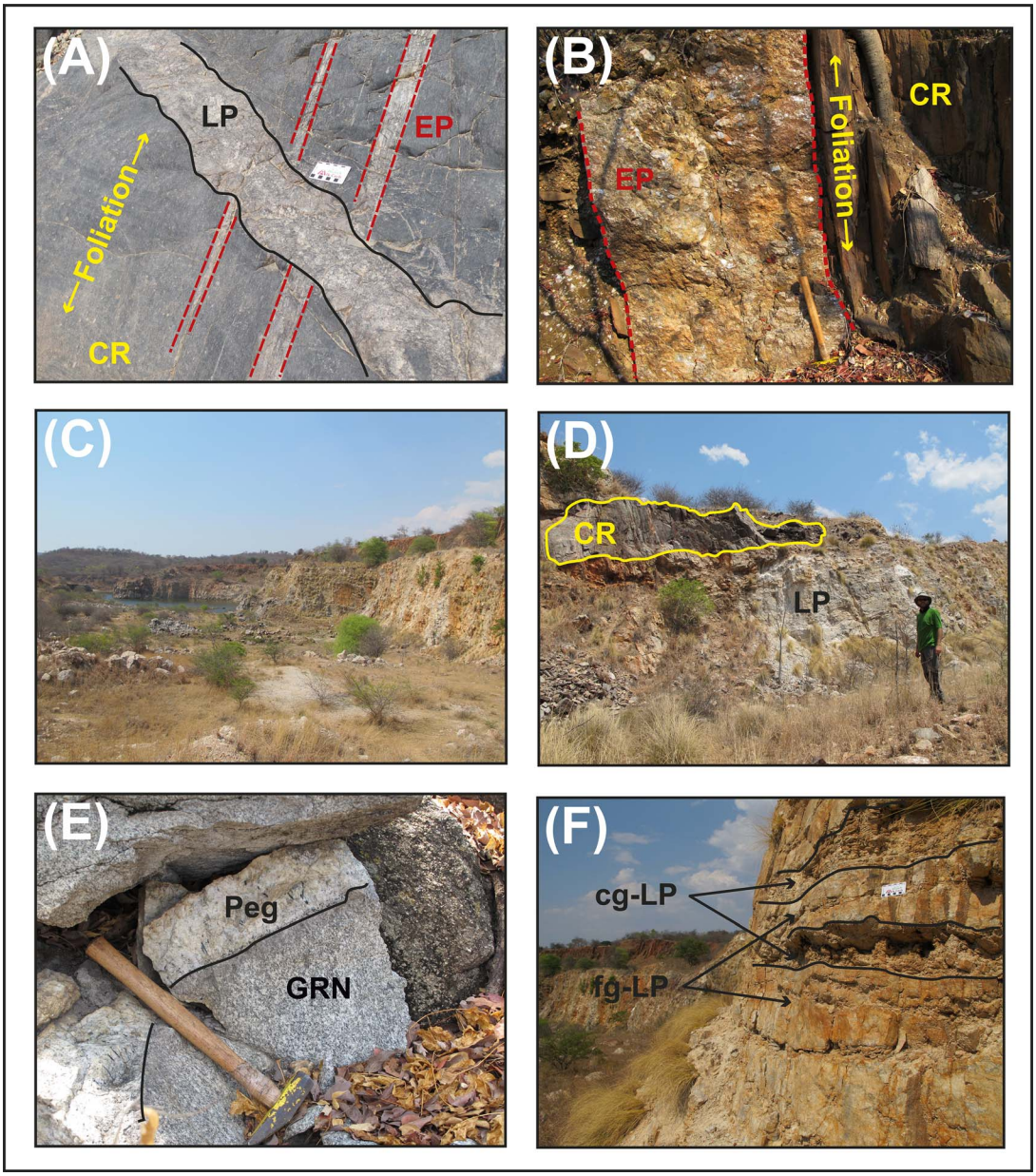

FIG. 3. Field photos from the Kamativi area. (A) Cross-cutting relationships in the Gwai River Gorge. Early pegmatites (EP) are deformed and parallel to the foliation; these are offset and cross-cut by an irregular late pegmatite (LP). Scale card is 10 cm long. (B) Early pegmatite (EP), parallel to the steeply dipping foliation in the country rocks (CR). (C) Overview of the old tin mine at Kamativi. Walls are *ca*. 20 m in height. (D) Exposure in the mine walls, with white pegmatite (LP) below and darker, grayish raft of country rock (CR) above. The country rock has a steeply dipping foliation (yellow arrow). (E) Pegmatite (Peg) intruding granite (GRN) at Kapami. (F) Banding in the pegmatite in the Kamativi tin mine, where fg-LP is fine-grained late pegmatite and cg-LP is coarse-grained late pegmatite.

selected for whole-rock geochemical analysis. Some very coarse-grained samples were recognized as not being suitable for whole-rock analysis, and country rocks were not analyzed because the small number of samples collected were not considered to be fully representative of the mineralogical variation observed in the field (Table 1).

Whole-rock geochemistry

Eighteen bulk-rock samples which were considered to be homogeneous enough to give meaningful whole-rock analyses were initially prepared at the British Geological Survey (BGS). Approximately 1 kg of each sample was jaw-crushed to a nominal grain size of 5

TABLE 1. SAMPLE LOCATIONS, COORDINATES, AND WORK CONDUCTED

Sample ID	Easting	Northing	Location	Rock type	Type	PTS	WRG	SEM-EDX (CGMs)	Phase mapping
ZIM_18_01	1141065	7962351	Kamativi Mine	Pegmatite	RF	Y	Y		Y
ZIM_18_02	1141088	7962278	Kamativi Mine	Schist	RF	Y			
ZIM_18_03	1141088	7962278	Kamativi Mine	Schist	RF	Y			
ZIM_18_04	1141088	7962278	Kamativi Mine	Greisen	RF	Y		Y	
ZIM_18_05	1141088	7962278	Kamativi Mine	Pegmatite	RF	Y	Y		
ZIM_18_06	1141104	7962259	Kamativi Mine	Aplite	RF	Y	Y		Y
ZIM_18_07	1141080	7962121	Kamativi Mine	Pegmatite	RF	Y	Y		
ZIM_18_08	1141080	7962121	Kamativi Mine	Pegmatite	RF	Y	Y		
ZIM_18_09	1141031	7962083	Kamativi Mine	Pegmatite	RF	Y	Y	Y	Y
ZIM_18_10	1140805	7962506	Kamativi Mine	Pegmatite	RF	Y	Y		
ZIM_18_11	1140524	7963352	Kamativi Mine	Pegmatite	RF	Y			
ZIM_18_12	1140524	7963352	Kamativi Mine	Pegmatite	RF	Y		Y	
ZIM_18_13	1140524	7963352	Kamativi Mine	Pegmatite	RF	Y			
ZIM_18_14	1140524	7963352	Kamativi Mine	Pegmatite	RF	Y		Y	
ZIM_18_15	1140524	7963352	Kamativi Mine	Pegmatite	RF	Y		Y	
ZIM_18_16	1140524	7963352	Kamativi Mine	Pegmatite	RF	Y	Y		
ZIM_18_17	1140524	7963352	Kamativi Mine	Pegmatite	RF	Y			Y
ZIM_18_18	1147858	7962519	Kalinda Mine	Schist	RF	Y			
ZIM_18_19	1147858	7962519	Kalinda Mine	Pegmatite	RF	Y			
ZIM_18_20	1148009	7962370	Kalinda Mine	Pegmatite	RF	Y			
ZIM_18_21	1148009	7962370	Kalinda Mine	Pegmatite	RF	Y			
ZIM_18_22	1147949	7963419	Kalinda Mine	Granitoid	RF	Y	Y		
ZIM_18_23	1118442	7951855	Kamativi roadcut	Granitoid	RF	Y	Y		
ZIM_18_24	1094885	7943753	RHA Mine	Schist	DC	Y			
ZIM_18_25	1094885	7943753	RHA Mine	Schist	DC	Y			
ZIM_18_26	1094885	7943753	RHA Mine	Pegmatite	DC	Y			
ZIM_18_27	1117097	7952976	Kapami granite quarry	Granitoid	RF	Y	Y		
ZIM_18_28	1117097	7952976	Kapami granite quarry	Pegmatite	RF	Y			
ZIM_18_29	1117155	7953041	Kapami granite quarry	Pegmatite	RF	Y	Y		
ZIM_18_30	1116979	7952860	Kapami granite quarry	Pegmatite	RF	Y	Y		
ZIM_18_31	1116171	7954844	Kapami roadcut	Schist	RF	Y			
ZIM_18_32	1138634	7960683	Gwai River Gorge	Schist	RF	Y			
ZIM_18_33	1138621	7960745	Gwai River Gorge	Aplite	RF	Y			
ZIM_18_34	1138621	7960745	Gwai River Gorge	Pegmatite	RF	Y	Y		
ZIM_18_35	1138621	7960745	Gwai River Gorge	Schist	RF	Y			
ZIM_18_36	1138621	7960745	Gwai River Gorge	Aplite	RF	Y	Y		
ZIM_18_37	1139698	7960648	Kamativi roadcut	Mafite	RF	Y			
ZIM_18_38	1139861	7960643	Kamativi roadcut	Pegmatite	RF	Y	Y		
ZIM_18_39	1140053	7964819	North of Kamativi Mine	Pegmatite	RF	Y			
ZIM_18_40	1140053	7964819	North of Kamativi Mine	Pegmatite	RF	Y			
ZIM_18_41	1139853	7964773	North of Kamativi Mine	Pegmatite	RF	Y			Y
ZIM_18_42	1139853	7964773	North of Kamativi Mine	Greisen	RF	Y			

PTS = polished thin section. WRG = whole-rock geochemistry. SEM-EDX (CGMs) = SEM energy dispersive X-ray analysis of columbite group minerals. RF = rock fragments. DC = drill core.

mm. The crushed material was split using a riffle splitter to produce a 30 g sub-sample. The sub-sample of riffled material was then milled to a grain size of about 32 μm using a planetary ball mill fitted with agate milling material. The milled powders were shipped to Bureau Veritas Minerals (Vancouver) for digestion and analysis.

The samples were analyzed for major oxides by X-ray fluorescence spectroscopy (procedure number: XF700) and a suite of 45 trace elements by inductively coupled plasma-mass spectrometry (ICP-MS), following decomposition of 0.2 g of sample by lithium borate fusion and dilute acid digestion (procedure number: LF100-EXT). Due to our interest in lithium, a separate 0.25 g aliquot of sample was decomposed by sodium peroxide and analyzed by inductively coupled plasma-atomic emission spectroscopy (ICP-AES) (procedure number: PF370-X) to give the total lithium abundance. Analyses of duplicate sample pairs are typically within 5% of each other for Rb, K, Cs, Li, Sr, Ba, P, Ti, Ga, Ta, Nb, Sn, Hf, Y, and Th and within 10% for Zr and U. Data for Be are very close to method detection limits and therefore have a poorer precision (>10%). Data for blanks are below method detection limits for all elements, and data for certified reference materials [SO-19, SY-4(D) and OREAS184] are in line with accepted values. All sample data, including quality control data, are included in Supplemental Table A[1].

Scanning electron microscopy (SEM)

Detailed mineralogical, petrographic, and microanalytical observations were made of polished thin sections (PTS) by backscattered electron (BSE) imaging using a Zeiss Sigma 300 field emission gun scanning electron microscope (FEG-SEM) fitted with twin Bruker X-flash energy-dispersive X-ray (EDX) detectors and running Zeiss' Mineralogic phase-mapping software (V 1.6.2). An electrically conductive coating was applied to the PTS prior to analysis as a thin film of carbon approximately 25 nm thick using an AGAR turbo carbon coater. Samples were examined under high vacuum conditions ($<10^{-4}$ Pa), at an accelerating voltage of 20 keV with a 120 μm aperture and 'beam boost' on to give a nominal beam current of 10 nA. Under these conditions, for select CGM crystals, EDX-based element maps were obtained in addition to BSE images, using Bruker Esprit software (V 2); these were collected at X-ray count rates of *ca*. 400 kcps for periods of greater than 20 min.

SEM phase mapping

Large area phase maps were produced using the Mineralogic system, with the SEM operating as above. Mapping was performed with beam step sizes of *ca*. 1–10 μm and per pixel dwell times of 10–80 ms. Phase identification was based on normalized, quantitative EDX data processed through expert-user-defined filters (based on element presence, absence, quantity, and key element ratios, *e.g*., Al:Si). Phase map images were produced by combining data from multiple adjacent fields of view to produce large-area mosaics covering PTS sample areas of 2 by 2 mm to 8 by 16 mm.

SEM quantitative microanalysis

Quantitative microanalysis was performed of select CGM crystals using an FEI Company Quanta 600 environmental SEM equipped with an Oxford Instruments INCA Energy 450 energy-dispersive X-ray microanalysis system with a 50 mm^2 Peltier-cooled silicon-drifted X-ray detector. The EDX system was fully calibrated for major element quantification [certified pure elements for Ta, Nb, Mn, and BGS' Fayalite standard (L136) for Fe]. Analyses were obtained from carbon-coated PTS with the following instrument conditions: high vacuum, 20 kV accelerating voltage, spot size 5 (equivalent to a beam current of 0.7 nA), 10 mm working distance, data acquisition live time of 30 s, X-ray process time 4, and 0–20 keV X-ray spectral range at a resolution of 10 eV/channel. Data were processed using INCA software (V 4.6), with oxygen quantified by stoichiometry (Fe valency set at 2). Analytical totals greater than 2 wt.% outside of 100 wt.% were discarded. Beam stability was monitored hourly using a Faraday cup, and drift was corrected where necessary by optimization with a pure Co standard.

Qualitative X-ray diffraction (XRD)

Qualitative XRD was primarily employed to positively identify fine-grained alteration phases (*e.g*., analcime and cookeite) found in the late pegmatites. Representative subsamples were ball-milled to reduce the grain size to <125 μm. Subsamples of the <125 μm material were micronized under acetone for 10 min using a McCrone micronizing mill for bulk-rock mineralogical identification. Bulk-rock XRD analysis was carried out using a PANalytical X'Pert Pro series diffractometer equipped

[1] Supplementary Data are available from the Depository of Unpublished Data on the MAC website (http://mineralogicalassociation.ca/), document "Kamativi Pegmatite, CM60, 21-00032".

with a cobalt target tube, X'Celerator detector, and operated at 45 kV and 40 mA.

Optical cathodoluminescence (CL)

The relationship between some mineral phases, for example spodumene and petalite, is difficult to elucidate using optical microscopy methods alone because the fine-grained nature of the petalite makes distinction of its optical properties very challenging. In these cases, optical CL was utilized to get a better understanding of the relationship between these phases (Fig. 6). Optical CL imaging was undertaken using uncoated, polished thin sections and a Technosyn CL 8200 Mk II cathodoluminescence system. Images were captured using an Axiocam MRC5 camera attached to a Nikon petrographic microscope.

Petrography and Mineralogy

Pelitic schists

The country rocks immediately around the Kamativi mine are typically well-banded quartz (*ca*. 40%) - biotite (*ca*. 20%) - muscovite (*ca*. 30%) pelitic schists, locally containing garnet and sillimanite. Tourmaline (*ca*. 5–10%) is common in the schists close to the contact with the late pegmatites and clearly overgrows the foliation (Fig. 4A), indicating that it was formed by metasomatism at the pegmatite margins.

Granitoids

Granitoids in the Kamativi area are coarse-grained and are characterized by their granoblastic texture and the rarity of primary magmatic crystal shapes. They comprise large (up to 4 mm), subhedral plates of variably sericitized alkali feldspar in a matrix of finer-grained recrystallized quartz, with some plagioclase, biotite, and minor muscovite. Mafic minerals, dominantly biotite, account for between 5 and 10% of the rock. Alkali feldspars are generally microperthitic and occasionally contain blebs of myrmekite. Some of the larger alkali feldspar plates are poikilitic and contain inclusions of quartz and biotite. Accessory minerals include apatite, ilmenite, monazite, zircon, minor xenotime, and large (up to 7 mm) complexly zoned allanite crystals. In places, an interesting micro-assemblage of symplectic monazite in apatite, mantled by poorly zoned allanite, is also observed. The accessory minerals are typically small ($<$50 μm) and occur as inclusions within biotite.

Early pegmatites

Early (unmineralized) pegmatites comprise coarse-grained muscovite mica (*ca*. 7 mm across), alkali feldspar ($>$10 mm across), and quartz, with minor garnet and variable amounts of zoned tourmaline. Accessory mineral phases include apatite, ilmenite, allanite, zircon, minor monazite, and very minor pyrite. Importantly, none of our early pegmatite samples contain cassiterite, nor do they contain lithium-bearing minerals such as spodumene. Alkali feldspars are generally perthitic and heavily sericitized, especially along their grain boundaries. Chloritization of muscovite mica is also common. Early pegmatites are typically strongly to very strongly deformed, with quartz, muscovite, and feldspar all exhibiting undulose extinction. Further evidence of deformation takes the form of kink-bands in curved muscovite crystals and offset twinning in some of the feldspars. Quartz is commonly recrystallized to granoblastic textures, locally forming elongate ribbons in the most highly strained samples (Fig. 4B).

Late pegmatites and aplites

The late pegmatites are typically poorly zoned; however, a clear distinction can be made between the margins of these intrusions and their cores. Samples taken from the unmineralized margins of the Main Kamativi Pegmatite comprise coarse-grained quartz (up to 10 mm across), plagioclase (up to 20 mm across), and variable amounts of muscovite (up to 10 mm long) and tourmaline (up to 9 mm long). Samples from the margins also show signs of strain, with many minerals exhibiting undulose extinction. Highly recrystallized quartz and heavily fractured tourmaline crystals provide additional evidence of deformation at the margins of the Main Kamativi Pegmatite. Samples from these marginal zones contain only very minor amounts of cassiterite, CGM, and lithium-bearing phases such as spodumene.

Even though the core of the Main Kamativi Pegmatite is not classically zoned, it does show some banding that comprises alternating layers of finer-grained aplitic material and coarser-grained bands. The coarse-grained bands mostly comprise large (up to 20 mm) subhedral plates of quartz and perthitic alkali feldspar in a matrix of finer-grained (typically between 0.5 and 2 mm) quartz, plagioclase, and muscovite. The coarse-grained bands also contain spodumene, montebrasite, cassiterite, CGMs (ferrocolumbite and ferrotantalite), and very minor amounts of beryl. Spodumene is the most abundant lithium mineral in the coarser-grained bands; however, the amount of spodumene can be highly variable, ranging between $<$5% in some of the most altered samples to $>$50% in samples that contain massive spodumene, alkali feldspar, and quartz. Spodumene generally takes the form of subhedral

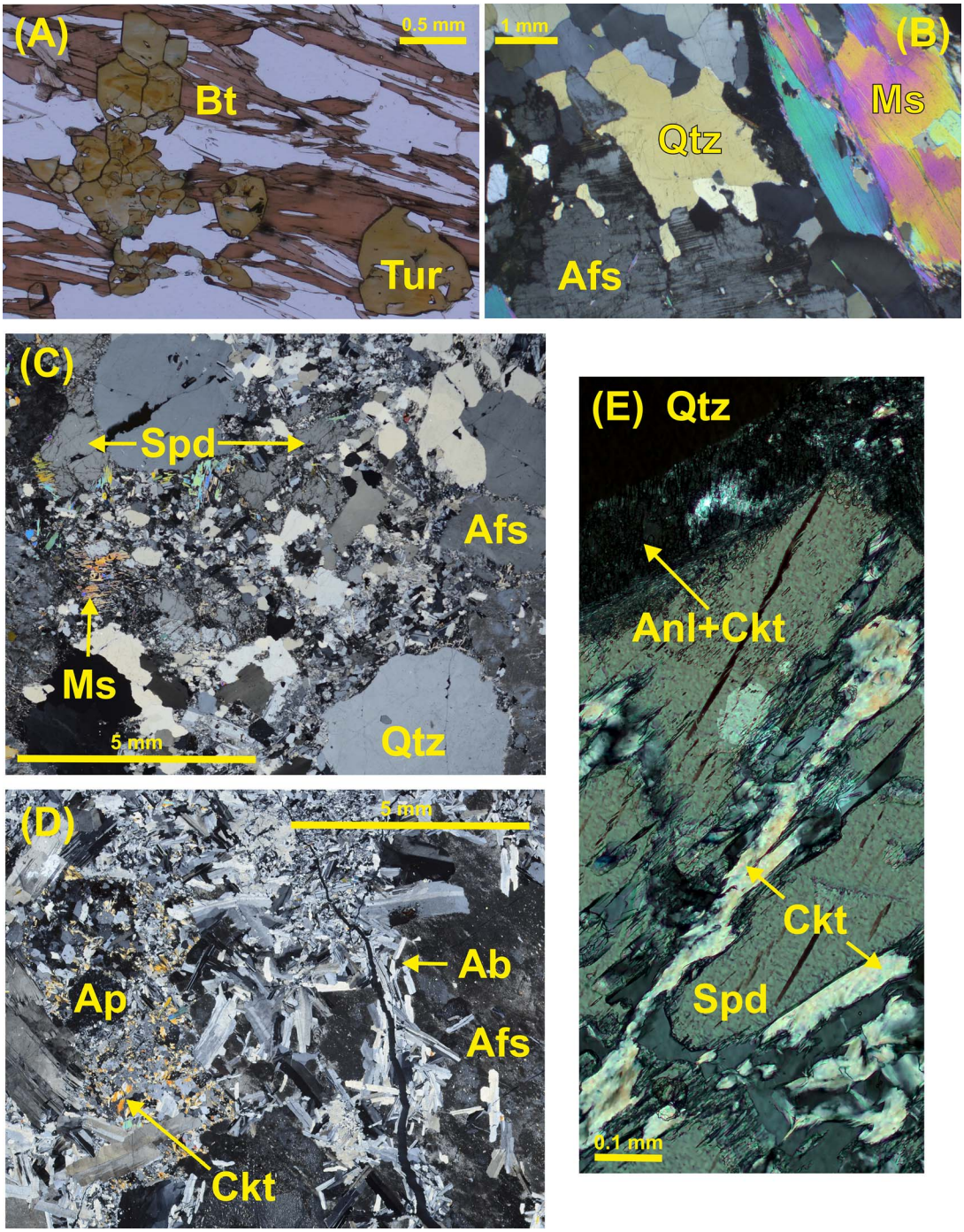

FIG. 4. Photomicrographs of (A) tourmaline-bearing pelitic schist from the Kamativi mine; (B) an early pegmatite from the Kalinda Mine; (C) a sample of spodumene-bearing pegmatite from the Kamativi mine; (D) a sample of partially albitized spodumene-bearing pegmatite; and (E) cookeite in fractures in a spodumene crystal. Mineral abbreviations from Mineralogical Association of Canada (2019), except "Afs", which is alkali feldspar.

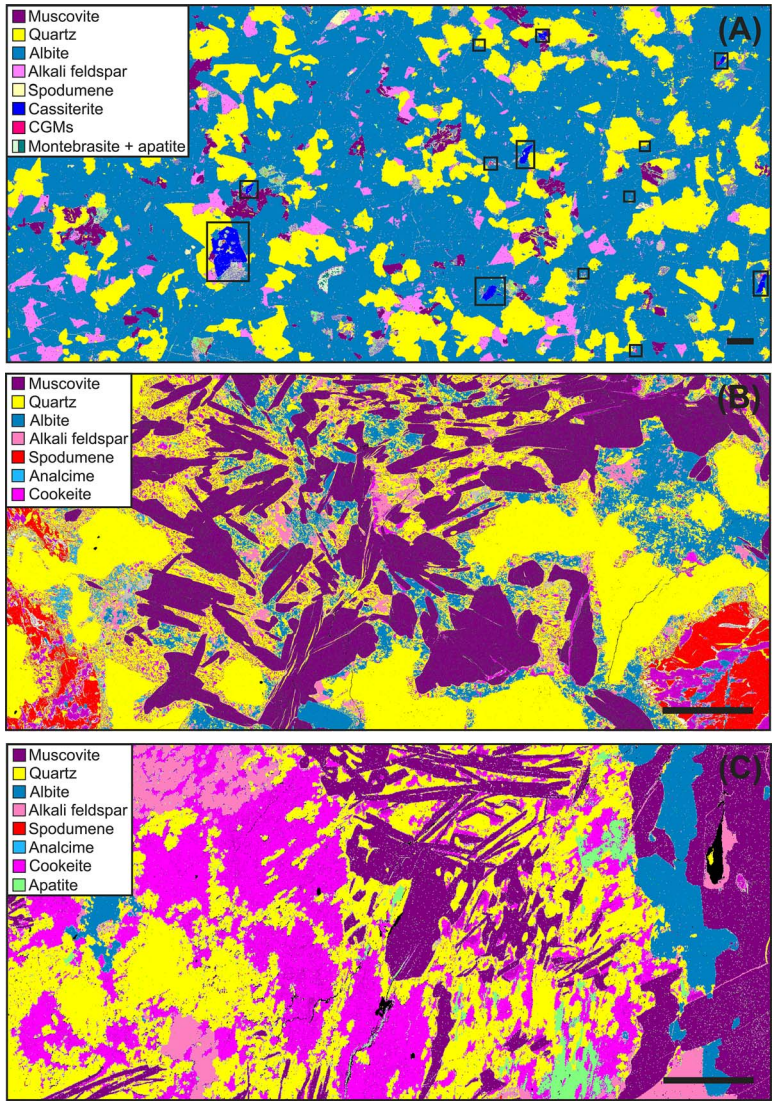

FIG. 5. False-colored SEM mineral phase maps showing the mineral assemblages associated with key stages in the paragenesis of the Main Kamativi Pegmatite. (A) Stage 2 albitization associated with the formation of cassiterite and CGMs. (B) Stage 3 muscovite-quartz (greisen) overprinting early lithium minerals. (C) Pervasive stage 4 hydrothermal alteration of earlier paragenetic stages (1–3). Scale bars are 500 μm. Black boxes highlight the location of cassiterite and CGMs.

plates up to 30 mm across in a matrix of finer-grained quartz and alkali feldspar (Fig. 4C), or as smaller (up to 10 mm across) crystals that appear to be interstitial to quartz and alkali feldspar. Montebrasite is also found in the coarse-grained quartz, alkali feldspar assemblage; however, it is much less common, typically accounting for <5% of the rock. It takes the form of subhedral crystals up to 5 mm across that display well-developed fine-twinning.

Another key characteristic of the coarse-grained bands is the presence of interlocking masses of bladed albite crystals (between 0.5 and 3 mm long) that take the form of veinlets that follow grain boundaries, or in cracks in alkali feldspar, spodumene, and quartz (Fig. 4D). Some of the larger albite crystals (up to 4 mm across) contain quartz inclusions that are aligned with crystallographic boundaries in the albite, indicating co-crystallization of these phases. Cassiterite and

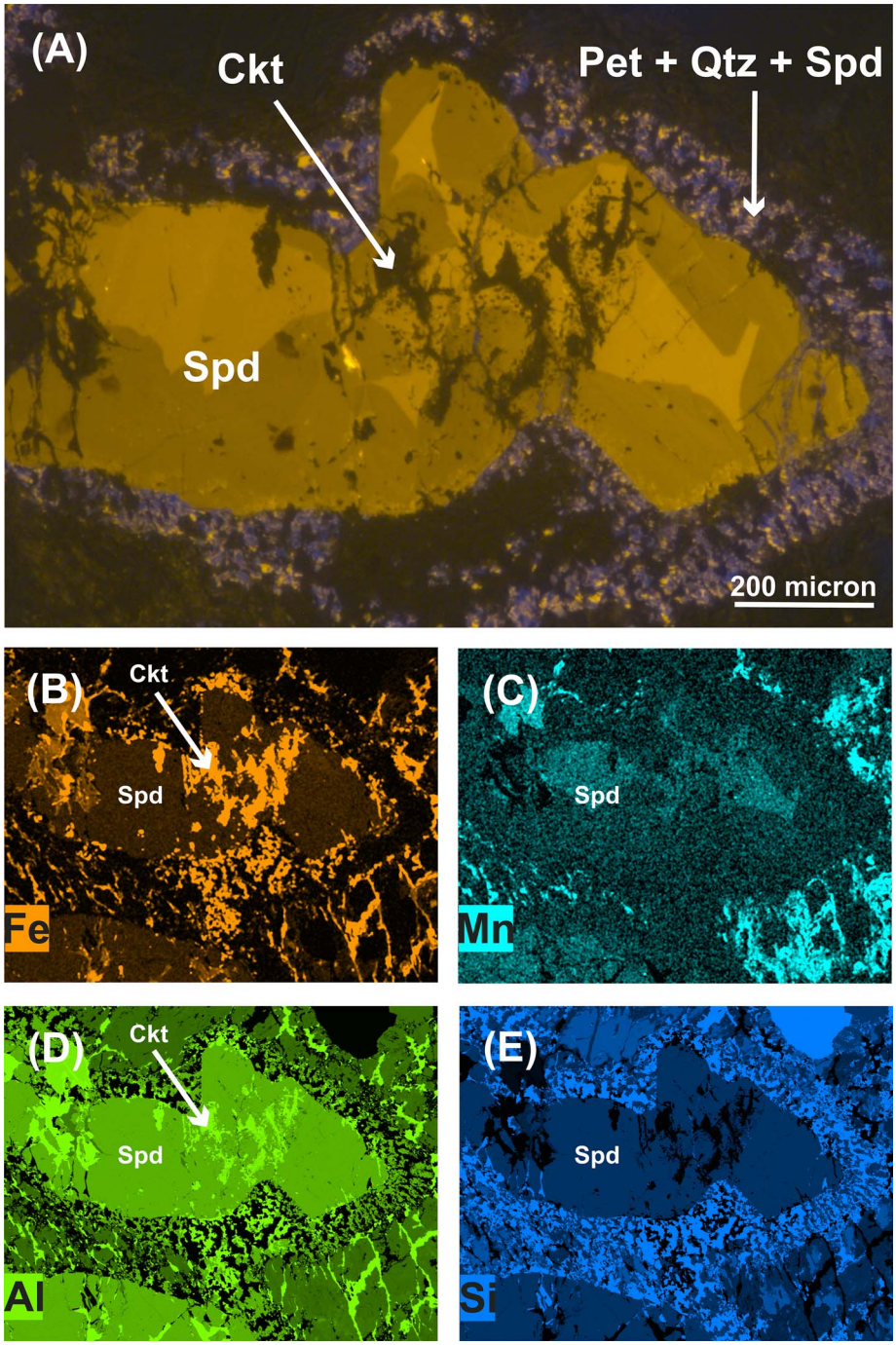

FIG. 6. (A) Optical cathodoluminescence (CL) image of a spodumene grain with a rim of fine-grained petalite + spodumene and quartz. (B) SEM-EDS Fe map showing low Fe in spodumene and petalite but high Fe in cookeite. (C) SEM-EDS Mn map showing high Mn in the core of the spodumene grain, which corresponds to the strong CL response. (D) SEM-EDS Al map showing subtle differences in Al content in petalite and spodumene. (E) SEM-EDS Si map highlighting the presence of quartz intergrown with spodumene. Mineral abbreviations from Mineralogical Association of Canada (2019).

CGMs are often associated with these albite-rich areas, either taking the form of inclusions in large albite crystals, or as interstitial crystals in a matrix of albite and quartz (Fig. 5A). Cassiterite tends to form euhedral, simply zoned crystals up to 500 μm long, whereas CGMs take the form of complexly zoned, acicular crystals up to 200 μm in length. In some cases, cassiterite and CGMs are very closely associated, with one phase partially encompassing the other.

Lithium minerals in the coarse-grained bands are variably altered. In some cases, alteration is confined to cleavage planes and grain boundaries; however, it can be more pervasive, leading to the almost complete breakdown of primary spodumene and montebrasite. Spodumene, alkali feldspar, and quartz in the coarse-grained bands are often replaced by an assemblage of fine-grained muscovite and quartz, which in some places contains fragments of unaltered spodumene (Fig. 5B). Locally, in some albite-rich samples spodumene has a very close association with petalite ($LiAlSi_4O_{10}$), particularly along grain boundaries and in fractures within primary spodumene crystals. The petalite is typically fine-grained and intergrown with spodumene and quartz. In some places minor cookeite and albite are also present in the assemblage. This relationship between spodumene and petalite is particularly difficult to elucidate because the fine-grained nature of the petalite makes determining its optical properties very challenging. Optical CL and SEM-EDS element mapping were utilized to better understand the relationship between spodumene and petalite. Under CL conditions, the spodumene displays a bright orange luminescence, whereas petalite can be readily distinguished under CL by its characteristic blue-purple luminescence. We carried out detailed analysis of a spodumene crystal that is surrounded by a rim of fine-grained, intergrown, quartz + spodumene + petalite (Fig. 6A). The SEM-EDS element maps show that the luminescence response of the spodumene is controlled by Fe and Mn, with Fe-rich areas having a much lower CL response compared to areas with high Mn (Fig. 6A and B). It is also notable that both fine-grained petalite and spodumene in the rim region generally have very low Fe and Mn contents (Fig. 6B and C). Although subtle, Al and Si maps further aid identification of these finely intergrown mineral phases, with spodumene typically having more Al and less Si compared to petalite (Fig. 6D and E). The quartz intergrown with petalite and spodumene is also readily picked out in the Si map (Fig. 6E). Interestingly, Fe- and Al-rich areas within the crystal correspond to the presence of non-luminescing cookeite (Fig. 6A and D). This intergrown rim clearly post-dates the central spodumene crystal, but it is not clear whether the relationship is one of replacement or overgrowth. Regardless of the mechanism, it is evident that petalite post-dates spodumene in the paragenesis at Kamativi.

Montebrasite also shows evidence of alteration, although the breakdown assemblage differs, being dominated by apatite and K-feldspar. The degree of alteration is similarly variable; in some cases, whole crystals are replaced by intergrowths of K-feldspar, quartz, cookeite, and apatite, whereas in others the replacement is confined to fractures and cleavage planes (Fig. 5C).

The finer-grained bands predominantly comprise albite (between 0.5 and 3 mm across) and quartz (about 1 mm across) with varying amounts of alkali feldspar and relict spodumene, although in general lithium minerals are less abundant in the finer-grained bands than in the coarser-grained equivalents. The finer-grained bands also contain minor amounts of montebrasite and an unidentified Na phosphate mineral and an Fe-Mn-Ca phosphate that may be triphylite. The phosphate phases also appear to be altered, particularly along fractures within the mineral grains. In places the albite-quartz assemblage has been greisenised (*i.e.*, replaced by extensive muscovite). Albite in these finer-grained bands typically occurs as interlocking masses of bladed crystals that have no preferred orientation, sometimes taking the form of veinlets that run along grain boundaries, or in cracks in alkali feldspar, spodumene, and quartz. Some of the larger albite crystals in the finer-grained bands contain quartz inclusions that are aligned with crystallographic boundaries in the albite, indicating co-crystallization of these phases. The finer-grained bands also contain abundant cassiterite (up to 2 mm across) and CGMs (about 0.5 mm long).

Later alteration of the muscovite-quartz assemblage is also observed in both the finer- and coarser-grained bands, particularly along grain boundaries and fractures. This later phase of alteration affects all minerals, with alkali feldspar being replaced by cookeite [$LiAl_4(Si_3Al)O_{10}(OH)_8$] and clays and relict spodumene by a complex intergrowth of cookeite and analcime ($NaAlSi_2O_6{\cdot}H_2O$) (Fig. 4E).

Cross-cutting late aplites, observed in the Gwai River Gorge, have a similar mineralogy to the finer-grained bands in the pegmatites, being dominated by fine-grained (typically 0.5 mm), interlocking bladed albite and quartz, with some interstitial muscovite. Late cross-cutting aplites also contain fine-grained (up to 1 mm across) euhedral cassiterite grains, tourmaline, and acicular CGMs, whereas lithium minerals (*e.g.*, spodumene and montebrasite) seem to be largely absent.

Columbite group mineral zonation and chemistry

Columbite group minerals can be extremely useful for understanding pegmatite evolution and thus detailed investigation of CGMs was carried out in five samples from the Main Kamativi Pegmatite.

Zonation patterns in CGMs in both the coarser- and finer-grained bands were observed using BSE imaging and EDS element mapping. They can be broadly categorized into three types: (1) progressive zonation, where there is a general change in composition from core to rim; (2) oscillatory zonation, where there are regular, alternating changes in composition; and (3) patchy zonation, where turbid, undulose zonation overprints progressive and oscillatory types (Fig. 7).

Progressive zonation is the most common zonation type seen in CGMs from the Main Kamativi Pegmatite; a gradual increase in Nb or Ta is observed from core to rim, which is mirrored by changes in the BSE brightness (Fig. 7A). Oscillatory zonation is also common; however, it is not as widespread as progressive zonation in CGMs from the Main Kamativi Pegmatite. Viewed in BSE, oscillatory zonation takes the form of alternating light and dark bands of varying thickness. The difference in back-scatter brightness is directly related to the Nb and Ta content of the zones, with brighter zones typically being more Ta-rich (Fig. 7B, C).

Patchy zonation is abundant in the Kamativi CGMs and typically overprints earlier progressive and oscillatory zonation types. It can take the form of resorption textures around the rims of some CGM grains, or as highly porous, micro-fractured irregular areas with very high back-scatter brightness (Fig. 7B, C). The high back-scatter brightness is related to the high Ta concentrations found in these areas. Where CGMs display patchy zonation there is often local alteration of the minerals surrounding the CGMs. For example, associated with some of the most turbid CGMs are secondary mineral assemblages that contain Fe-oxides, apatite, cookeite, and kaolinite. In some cases, fractures running through the CGMs are infilled with kaolinite and/or cookeite. Columbite group minerals in the Main Kamativi Pegmatite have a wide range of Nb_2O_5 and Ta_2O_5 contents, ranging from 20.30 to 68.26% and 12.8 to 63.2%, respectively. The FeO (0.90 to 14.16%) and MnO (4.82 to 17.6%) contents also vary, but to a lesser extent. These ranges are also reflected in the Ta/(Ta + Nb) and Mn/(Mn + Fe) ratios, with the latter typically having a narrower range of values. That is, Mn/(Mn + Fe) ratios, with the exception of a few points that sit in the manganocolumbite field, are mostly in the range 0.14 to 0.45, whereas Ta/(Ta + Nb) ratios range from 0.1 to 0.65. However, overall compositions are dominated by Fe and Nb, with the majority of data points plotting in the ferrocolumbite field of the CGM quadrilateral diagram (Fig. 8). Data points that plot in the ferrotantalite field are typically associated with areas of patchy zonation and higher Ta concentrations. Similar compositional trends are observed in CGMs from pegmatites in the Cape Cross-Uis region of Namibia, where Ta/(Ta + Nb) ratios typically have a wider spread of values (0.06 to 0.98) than the Mn/(Mn + Fe) ratios (0.20 to 0.94) (Fuchsloch *et al*. 2019). Tin (SnO_2) concentrations in the Kamativi CGMs attain 2.09%, although the majority are typically <0.5%. There is a weak positive correlation between Sn and Ta, where the highest concentrations of Sn are associated with high concentrations of Ta. The opposite is observed for Nb, where high Sn concentrations are associated with lower concentrations of Nb. No correlation is observed between Sn and Fe, nor between Sn and Mn.

Mineral paragenesis

These petrographic studies allow identification of four main paragenetic stages associated with the formation of the core of the Main Kamativi Pegmatite. Although each stage in the paragenesis is marked by a characteristic mineral assemblage, the first three stages should be viewed as a continuous transition from magmatic-fluid to magmatic-hydrothermal conditions as part of an evolving system (Fig. 9). The four key stages are: (1) crystallization of a coarse-grained assemblage dominated by quartz, alkali feldspar, spodumene, and montebrasite; (2) partial alteration of assemblage 1 by widespread albitization, resulting in the formation of an albite, quartz assemblage containing cassiterite, CGMs, and relic spodumene and montebrasite (Fig. 5A); (3) irregular development of a quartz-muscovite greisen, CGM assemblage that partially replaces early spodumene, albite, and quartz (Fig. 5B); and (4) widespread fluid-induced alteration of earlier phases resulting in the formation of cookeite, sericite, analcime, and apatite (Fig. 5C). During stage 4, earlier formed CGMs were partially altered to more Ta-rich compositions, with the development of patchy zonation.

Whole-Rock Chemistry

All samples are granitic in composition with SiO_2 values typically more than 70 wt.% (Table 2). In general, all aplites and pegmatites in the Kamativi area have low MgO and TiO_2 contents (typically <0.5 wt.%) and low CaO and Fe_2O_3 contents (typically <2 wt.%), whereas concentrations of these oxides in granitoid samples are typically higher. Generally, Na_2O is the dominant alkali in the late pegmatites and aplites, whereas in samples of early pegmatite and

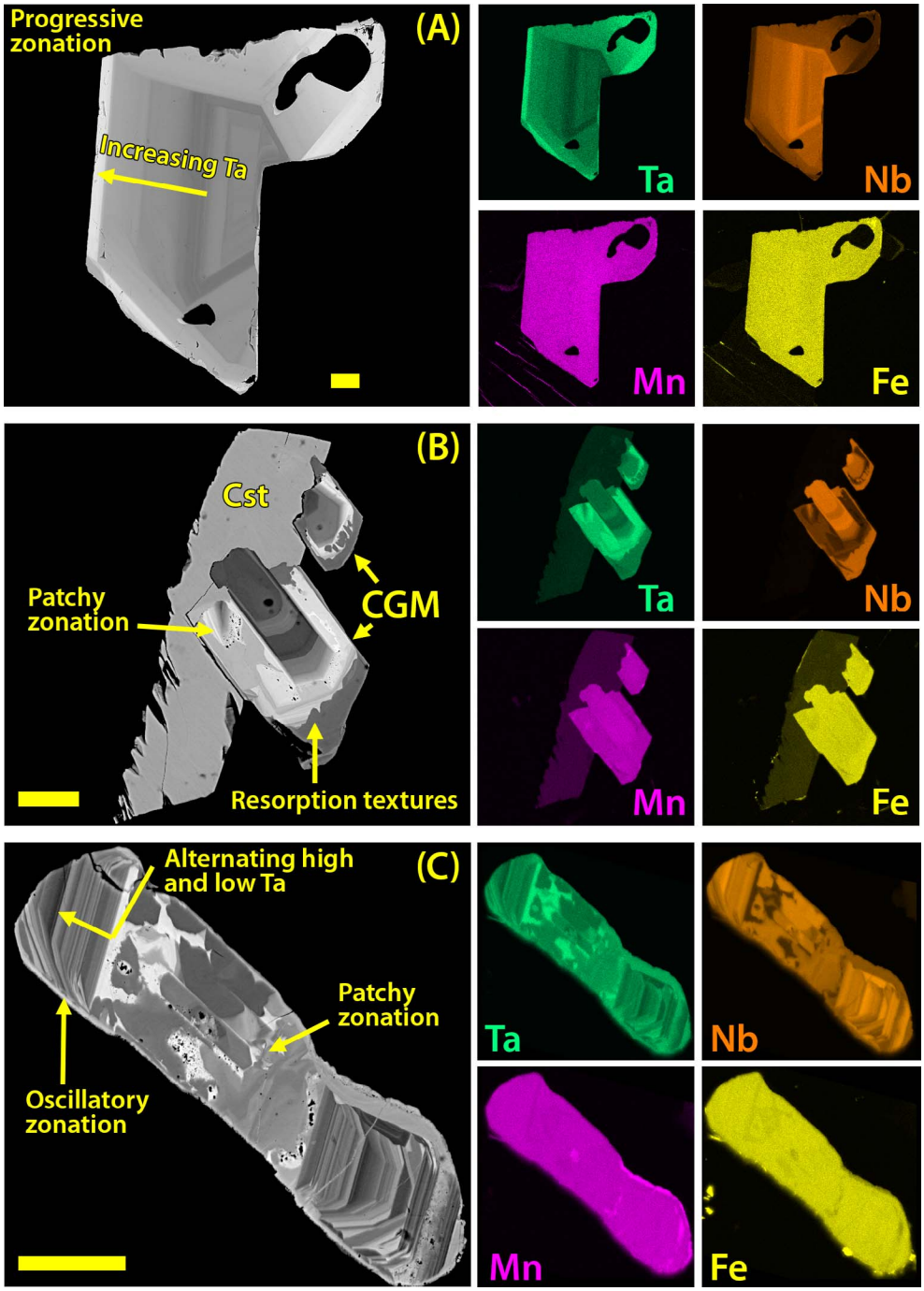

FIG. 7. SEM-BSE images of CGMs with associated element maps, showing (A) progressive zonation with a general increase in Ta from core to rim; (B) patchy zonation with localized enrichment in Ta; and (C) patchy and oscillatory zonation patterns in a single CGM grain. Scale bars are 20 μm.

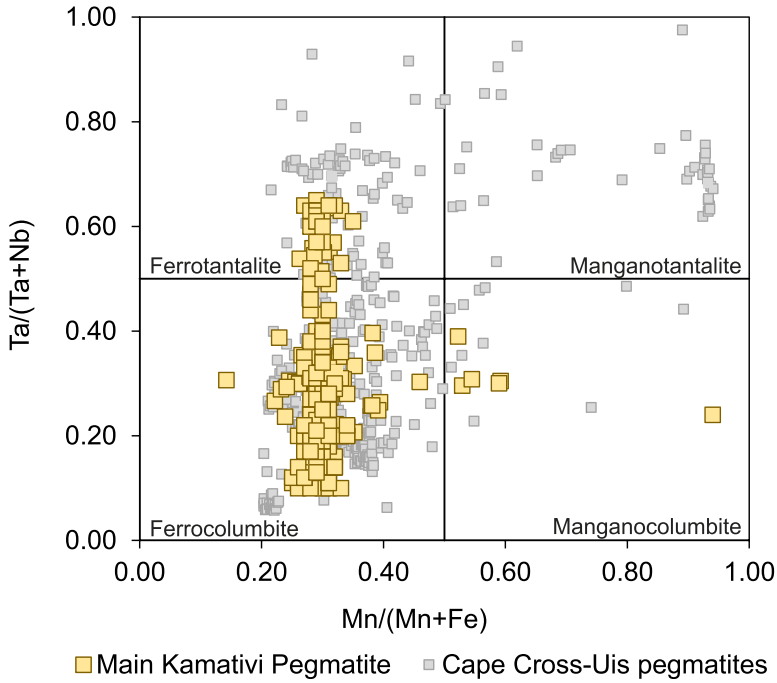

FIG. 8. CGM quadrilateral plot showing the range of compositions of CGMs from the Main Kamativi Pegmatite. Gray squares are data from the Cape Cross-Uis pegmatite belt in Namibia included for comparison (Fuchsloch *et al*. 2019).

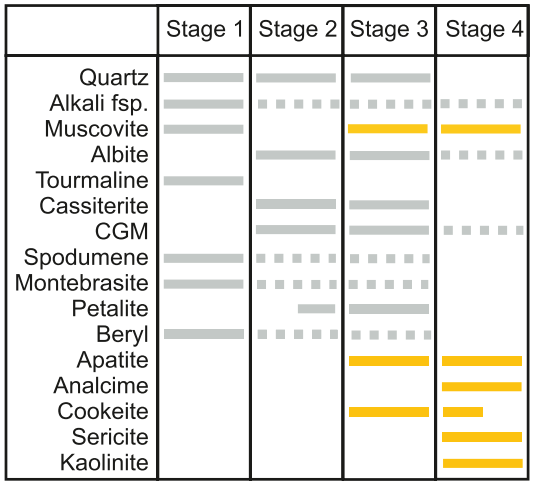

FIG. 9. Paragenesis diagram for the Main Kamativi Pegmatite showing the four key stages in the development of the pegmatite, including Stage 1 crystallization of spodumene, quartz, and alkali feldspar; Stage 2 albitization and the formation of cassiterite and CGMs; Stage 3 greisenisation (quartz-muscovite) replacing earlier formed phases; and Stage 4 late-stage hydrothermal alteration of earlier phases to form cookeite, apatite, zeolite, and clays. Dashed lines indicate alteration/breakdown of a mineral phase. Orange lines indicate secondary mineral phase.

in the granitoids K_2O is typically more dominant; this clearly reflects the greater abundance of albitic feldspar in the late pegmatites and aplites. Concentrations of P_2O_5 are also highest (up to 1.10 wt.%) in samples of late pegmatite and aplite. Similarly, loss on ignition values are also typically highest in samples of late pegmatite and aplite (up to 1.3%), which likely reflects the abundance of clay and zeolite minerals associated with the alteration of primary lithium minerals.

On a modified alumina saturation index (ASI) plot (Fig. 10), which includes lithium, all samples are peraluminous (A/CNKL $>$ 1.0). However, the majority are strongly peraluminous, having A/CNKL $\geq$ 1.2. Samples that deviate slightly from the peraluminous trend are samples of biotite-rich granitoid, which typically have a higher value of A/NKL for any given value of A/CNKL, likely driven by the abundance of potassium-rich mineral phases (*e.g*., biotite and K-feldspar) in these samples. A similar bifurcating trend is observed in pegmatite samples from northwest Scotland, where biotite- and K-feldspar-rich (barren) pegmatites have higher values of A/NKL at any given value of A/CNKL, whereas rare-metal pegmatites, that do not contain biotite or K-feldspar, are typically more peraluminous (Fig. 10) (Shaw *et al*. 2016).

TABLE 2. SUMMARY OF WHOLE-ROCK GEOCHEMISTRY FOR GRANITOIDS (GRN), EARLY PEGMATITES (EP), LATE PEGMATITES (LP), THE MARGINS OF THE MAIN KAMATIVI PEGMATITE (LPm), AND APLITES (AP)

Sample	22	23	27	10	30	34	38
Type	GRN	GRN	GRN	EP	EP	EP	EP
Oxide (wt.%)							
SiO_2	75.04	68.91	72.90	76.02	70.02	74.35	77.72
Al_2O_3	13.73	15.02	13.97	15.57	15.38	14.62	12.52
Na_2O	3.01	3.12	2.71	3.33	2.20	4.19	2.24
K_2O	5.36	3.72	5.16	2.38	9.82	4.68	6.20
CaO	1.05	2.87	1.75	0.82	1.05	1.14	0.78
MgO	0.27	1.11	0.66	0.19	0.06	0.08	0.08
P_2O_5	0.10	0.18	0.06	0.05	0.71	0.15	0.03
TiO_2	0.13	0.58	0.16	0.06	0.03	0.03	0.04
Element (ppm)							
Li	20	20	70	70	<10	30	<10
Cs	3.8	2.9	18.7	8.1	0.8	120.6	11.9
Rb	208.5	165.0	130.1	69.9	194.7	394.7	146.4
Sr	72.9	271.8	329.5	171.5	198.0	94.9	151.2
Ba	454	778	1025	549	1895	240	987
Ga	13.2	16.4	11.3	11.1	9.6	15.9	8.4
Ta	1.2	1.6	0.8	1.7	0.7	5.6	0.8
Nb	8.2	17.7	11.8	3.7	2.4	5.3	1.7
Be	3	<1	<1	15	<1	10	2
Sn	4	2	2	18	1	13	6
Hf	3.1	4.7	6.2	0.2	0.4	0.8	3.4
Zr	96.2	168.4	188.0	4.6	12.7	0.8	110.5
Y	38.8	7.7	18.3	2.8	41.1	18.0	6.1
Th	23.0	13.0	52.6	0.7	2.4	12.1	5.4
U	15.1	9.1	4.6	0.4	1.1	2.2	5.9
TREE	169.5	223.2	346.4	12.2	93.3	92.9	30.0

TREE is $\sum$La-Lu.

Granitoid samples from the Kamativi area are characterized by compositions that are relatively similar to those of bulk continental crust (Rudnick & Gao 2003) with slightly higher Cs (up to 18.7 ppm, average 8.5 ppm), Th (up to 52.6 ppm, average 30 ppm), and U (up to 15.1 ppm, average 9.6 ppm) (Fig. 10A). Samples of early pegmatite are distinguished from the granitoids by their higher contents of Ta (up to 5.60 ppm, average 2.2 ppm), Be (up to 15.0 ppm, average 6.9 ppm), and Sn (up to 18.0 ppm, average 9.5 ppm) and their lower contents of Ti (up to 0.060%, average 0.040%), Nb (up to 5.30 ppm, average 3.3 ppm), Hf (up to 3.40 ppm, average 1.2 ppm), and Zr (up to 111 ppm, average 36 ppm) (Fig. 11B). The late pegmatites and aplites have very high concentrations of Cs (up to 300 ppm, average 177 ppm), Li (up to 1.398%, average 0.29%), Ta (up to 175 ppm, average 120 ppm), and Sn (up to 1858 ppm, average 960 ppm), particularly in the samples from the mineralized cores; concentrations of these elements is lower in samples from the marginal zones. This enrichment generates pronounced positive anomalies for Cs, Li, P, Ta, and Sn and strong negative anomalies for elements such as Sr, Ba, Ti, Nb, Zr, Y, and Th on trace element plots normalized to continental crust (Fig. 11C).

Total rare earth element (TREE) concentrations are highest, and most consistent, in samples of granitoid (ranging between 169 ppm and 346 ppm, average 246 ppm). They have a relative enrichment in the light rare earth elements compared to the heavy rare earth elements and shallow negative Eu anomalies. In contrast, the TREE concentrations in samples of early pegmatite are typically lower, reaching a maximum of 93.3 ppm (average 57 ppm). Early pegmatites typically have flatter rare earth element (REE) patterns and variable Eu anomalies. Samples of late pegmatite and aplite have the lowest TREE contents, with most individual REE values being less than ICP-MS method detection limits. The TREE concentrations in these samples attain 14.5 ppm (average 3.3 ppm); however, most are less than 1 ppm. The REE patterns for samples of late pegmatite and aplite are gently sloping

TABLE 2. CONTINUED.

Sample	1	5	6	9	16	29	7	8	36
Type	LP	LP	LP	LP	LP	LP	LPm	LPm	AP
Oxide (wt.%)									
SiO_2	73.77	72.19	71.96	69.06	73.20	72.21	78.88	73.35	68.77
Al_2O_3	17.82	16.64	17.46	18.60	15.60	16.01	12.53	15.29	17.95
Na_2O	1.44	5.30	5.30	6.92	6.87	4.04	4.11	6.34	6.21
K_2O	2.82	2.21	2.68	3.03	2.06	4.57	1.67	0.77	5.35
CaO	0.09	0.46	0.15	0.42	0.61	0.66	0.74	0.49	0.59
MgO	0.05	0.10	0.04	0.09	0.04	0.05	0.15	0.32	0.05
P_2O_5	0.20	0.89	0.62	0.44	0.66	1.10	0.48	0.25	0.52
TiO_2	0.01	<0.01	0.01	<0.01	<0.01	0.01	0.05	0.04	0.02
Element (ppm)									
Li	13,980	3,360	1,010	1,140	330	310	200	130	20
Cs	190.3	155.5	300.1	152.7	111.8	160.0	46.2	16.6	167.4
Rb	>1000	>1000	>1000	>1000	>1000	>1000	271.3	186.0	841.4
Sr	10.7	76.7	71.6	70.6	60.7	49.1	80.7	13.7	44.7
Ba	3	10	10	60	15	113	47	21	90
Ga	15.9	22.4	31.9	20.8	21.5	21.7	11.6	9.8	33.4
Ta	17.5	115.9	175	174.8	79.1	118.4	2.0	0.7	159.9
Nb	23.3	124.4	92.3	131.0	75.5	107.7	6.8	1.3	109.9
Be	73	174	115	117	161	140	4	5	170
Sn	429	1451	930	932	1858	215	42	8	905
Hf	0.4	2.0	3.0	3.9	1.9	3.1	<0.1	0.1	3.1
Zr	3.2	12.4	19.7	25.4	15.4	24.3	1.7	4.0	18.4
Y	0.5	0.4	0.2	1.1	0.3	1.8	2.7	5.4	3.4
Th	<0.2	<0.2	<0.2	0.3	<0.2	1.1	0.3	<0.2	<0.2
U	2.1	5.3	6.0	5.7	5.8	3.1	1.6	0.7	4.9
TREE	0.560	0.570	0.250	0.760	0.500	14.5	5.08	6.10	5.80

to flat and lack observable Eu anomalies. They are also less consistent (*i.e.*, noisy) when compared to the REE patterns for samples of granitoid and early pegmatite; this is likely due to the extremely low concentrations of the individual REE measured in these samples (Fig. 12).

Sample groups can be readily distinguished on a ratio plot of Mg/Li *versus* La/Ta. Samples described as barren or unmineralized tend to plot in the unmineralized field, as they typically have high Mg/Li and La/Ta ratios. Samples of granite also plot in this field. Mineralized pegmatite samples typically have very low Mg/Li and La/Ta ratios and plot in either the Li-mineralized field or the Ta-mineralized field, depending on whether or not they are dominantly Li-mineral-bearing or CGM-bearing. Samples from Tres Arroyos on the Iberian Peninsula described as "intermediate pegmatites" largely plot in the Ta mineralized field, which can be explained by the dominance of CGMs over Li-minerals in these samples (Garate-Olave *et al*. 2020). Granitoid samples from the Kamativi area typically have the highest Mg/Li ratios (81–335) and La/Ta ratios (31–103), which reflects the general absence of Li- and Ta-bearing phases in these samples, and the presence of rare earth element-bearing phases such as monazite and allanite. In comparison, samples of early unmineralized pegmatite tend to have slightly lower Mg/Li (16–97) and La/Ta (1.6–18) ratios, reflecting the dominance of muscovite over biotite and the presence of Ta-bearing CGMs in these samples. Samples of late mineralized pegmatite and aplite contain Li-minerals (*e.g.*, spodumene) and abundant Ta-rich CGMs, resulting in very low Mg/Li ratios (typically <1) and very low La/Ta ratios (typically <0.5). Data for unmineralized pegmatites and granite from South Harris, Scotland (Shaw *et al*. 2016), have been added for comparison. Data for two large, composite samples from the Mt. Mica pegmatite, in Maine, USA (Simmons *et al*. 2016), and samples of granite, unmineralized (barren) pegmatite, and mineralized pegmatite from the Iberian Peninsula have also been added (Llera *et al*. 2019, Garate-Olave *et al*. 2020). However, full-suite bulk-geochemical data for individual samples are often not available

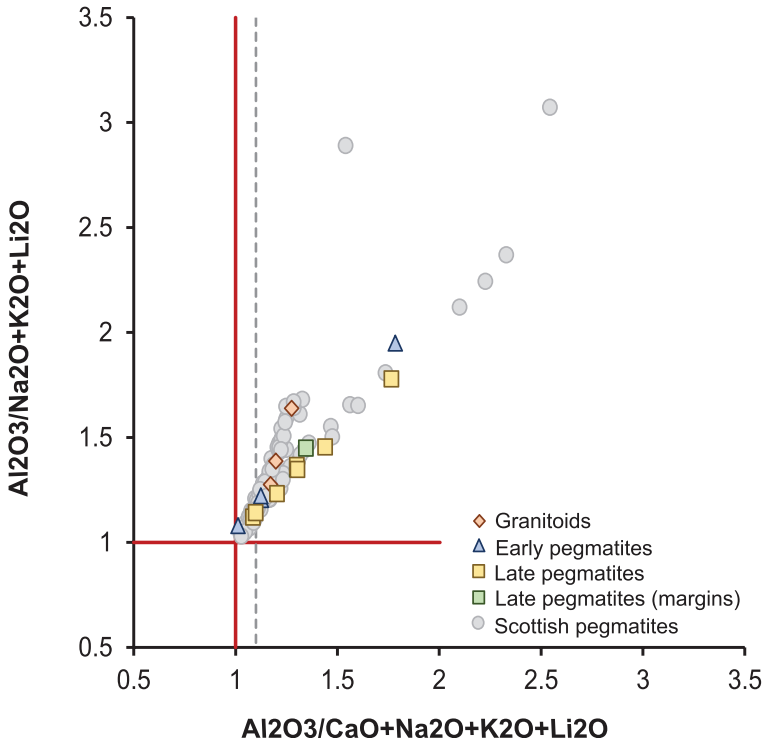

FIG. 10. Modified ASI plot showing the bifurcating trends between biotite-rich granitoid and peraluminous pegmatites in the Kamativi area. Gray circles are data from the NW Highlands of Scotland which show a similar bifurcating trend in pegmatite chemistry (*i.e.*, muscovite-garnet pegmatites *versus* biotite-magnetite pegmatites) (Shaw *et al*. 2016).

(*e.g.*, Li data are not available for granite from the Sebago Pluton in Simmons *et al*. 2016) for rare-metal pegmatites, making comparisons with other rare-metal pegmatites globally a challenge (Fig. 13).

DISCUSSION

Relative timing of magmatic events in the Kamativi area

We used a combination of field data and published dating to develop a timeline (Fig. 14) for the magmatic events in the Kamativi area. The first significant magmatic event was the emplacement of the granitoid plutons of the Dete-Kamativi inlier at 2080–2010 Ma (Glynn *et al*. 2020). These are foliated biotite granites and granodiorites, which have been interpreted as the roots of a magmatic arc that was emplaced prior to the Magondi Orogeny (Master *et al*. 2010, Glynn *et al*. 2020).

The early pegmatites are typically parallel to the foliation in their host rocks, with foliated margins, but in some cases appear to cross-cut the foliation at a low angle. In zones of more intense deformation, such as the Gwai River Gorge, they are pervasively deformed and transposed into the foliation. These pegmatites have not been studied by absolute dating methods. However, their field relationships are most consistent with emplacement toward the end of the major deformation event in their host rocks, namely the Magondi Orogeny. The presence of localized, low-angle cross-cutting relationships, and the preservation of igneous textures even in these relatively small intrusions, would not be consistent with emplacement of the pegmatites prior to the main deformation event. It is possible that the early pegmatites are genetically related to the later phases of the local granitoid plutons. The early pegmatites have lower REE contents than the granitoids, but in peraluminous systems where REE minerals such as monazite have fractionated early, the most evolved melts may be REE-poor (Bea *et al*. 1994). Accessory minerals such as allanite and monazite do occur in the granitoid plutons of the Dete-Kamativi inlier. It is thus difficult to distinguish for certain whether the early pegmatites were formed by melting of local crustal sources toward the end of the Magondi Orogeny or as the most evolved melts from the granitoid plutons.

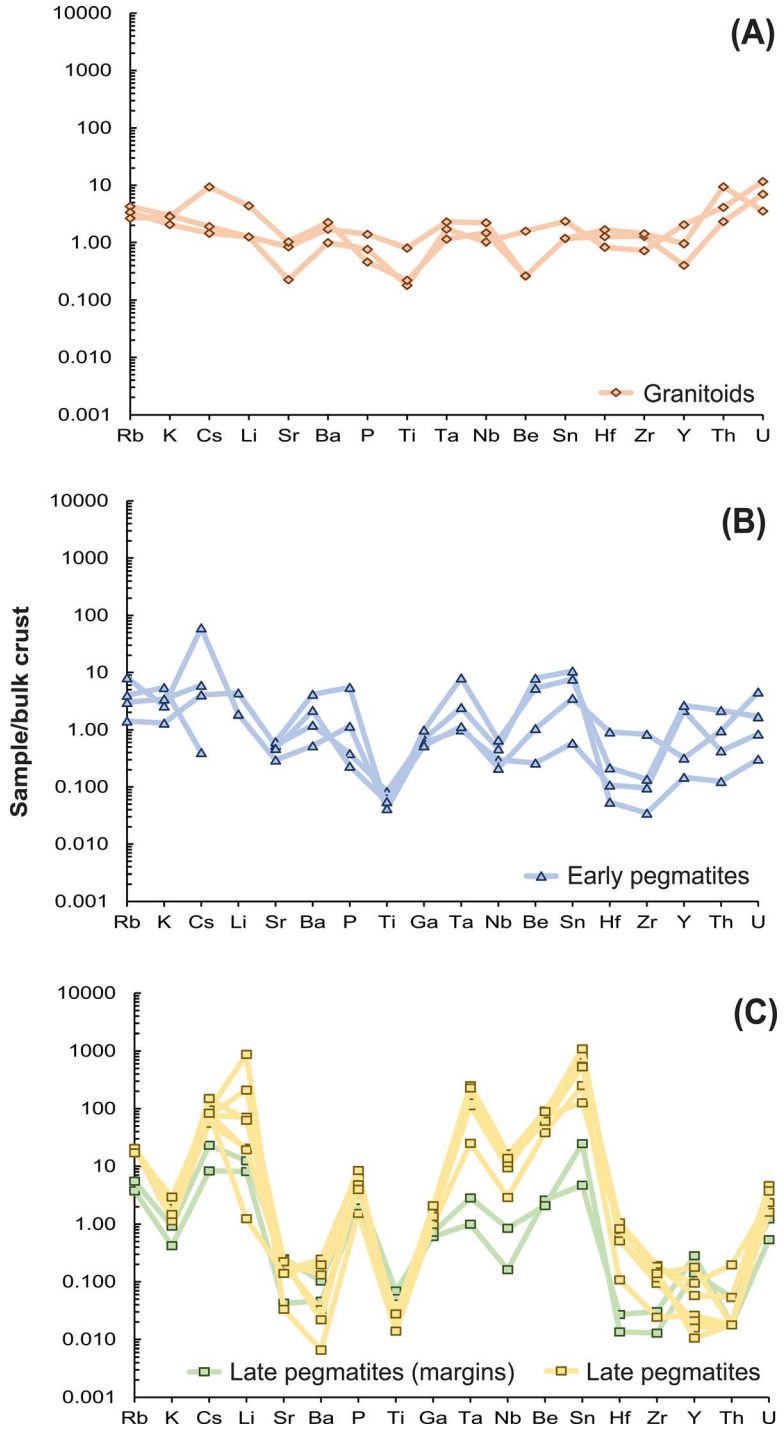

FIG. 11. Bulk continental crust normalized multi-element plots for (A) granitoids; (B) early pegmatites; and (C) late pegmatites in the Kamativi area. Normalizing factors from Rudnick & Gao (2003).

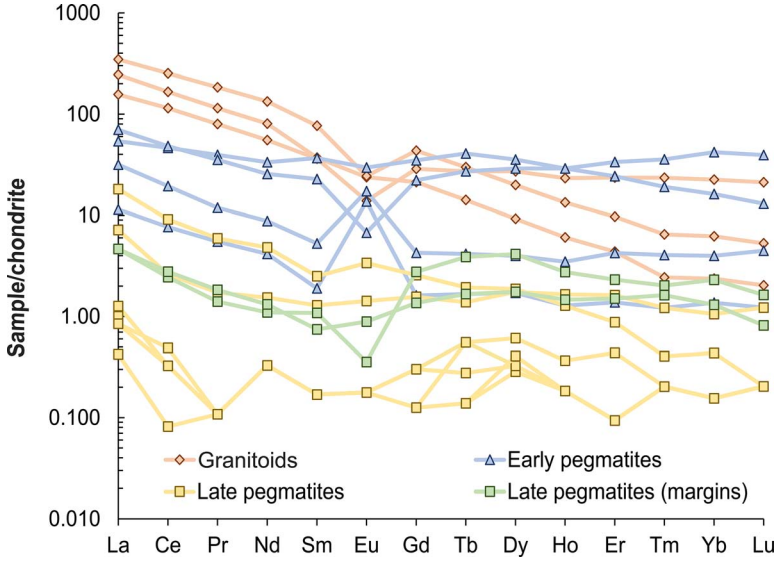

FIG. 12. Chondrite-normalized REE plots for (A) granitoids; (B) early pegmatites; and (C) late pegmatites in the Kamativi area. Normalizing factors from McDonough & Sun (1995).

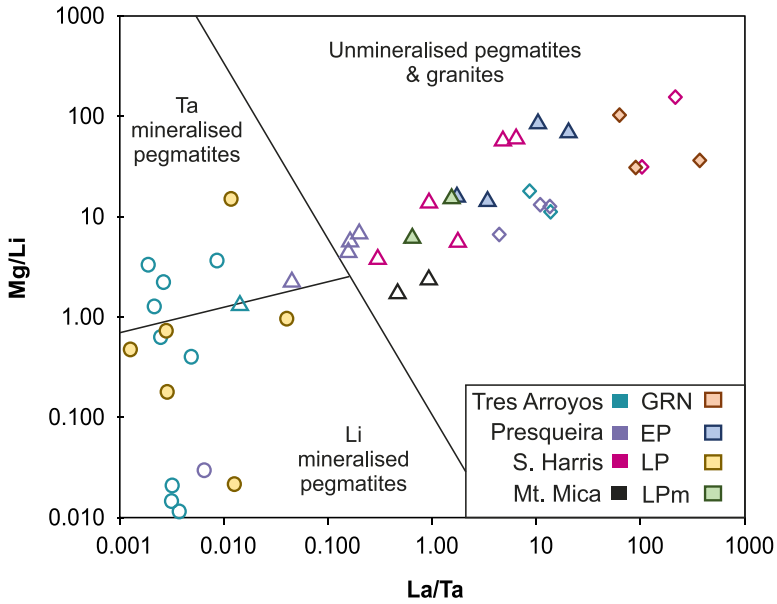

FIG. 13. Bulk rock Mg/Li *versus* La/Ta plot showing relative differences in Mg-Li-La-Ta concentrations between granitoids (GRN), early pegmatites (EP), late pegmatites (LP), and the margins (LPm) of the Main Kamativi Pegmatite. The late mineralized pegmatites have much higher Li and Ta contents compared to the more Mg and La-rich granitoids, early unmineralized pegmatites, and samples from the margins of the Main Kamativi Pegmatite. Data for unmineralized (barren) pegmatites are represented by triangles, diamonds are data for samples of granite, and circles are data for either Ta- or Li-mineralized pegmatites. Data (black triangles) from the Mt. Mica Pegmatite in North America (Simmons *et al*. 2016). Purple symbols are data from the Presqueira Pegmatite in NW Spain (Llera *et al*. 2019). Bright pink symbols are data from unmineralized pegmatites on South Harris, Scotland (Shaw *et al*. 2016). Turquoise symbols are data for samples from the Tres Arroyos Pegmatite in Spain (Garate-Olave *et al*. 2020).

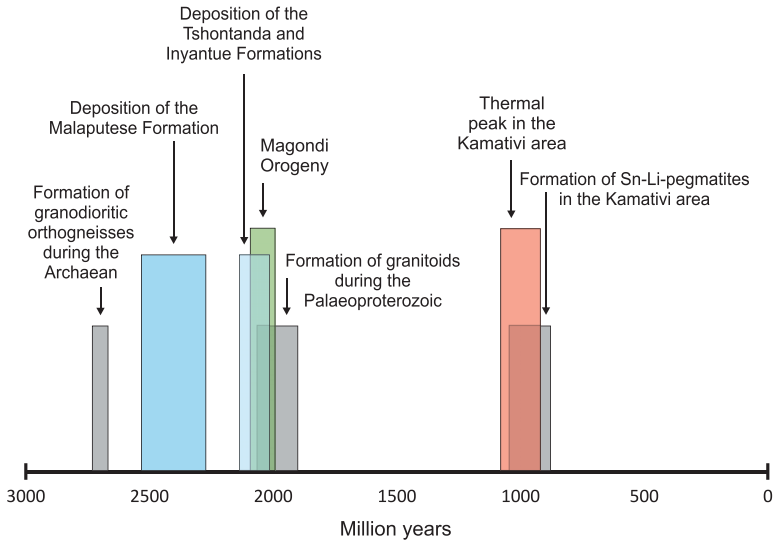

FIG. 14. Geochronology timeline showing key events in the Kamativi area. Ages from Glynn (2017) and Glynn *et al*. (2017, 2020).

The late pegmatites and associated aplites are distinct in terms of their field relationships. They form near flat-lying sheets that have sharp, clear cross-cutting relationships with the foliation in the host rocks, with very little disruption of those host rocks. This evidence indicates passive emplacement of the late pegmatites into brittle fractures, suggesting that the pegmatites are post-tectonic in nature. The field evidence is entirely consistent with the dating (U-Pb in coltan) of these pegmatites at 1030 ± 8 Ma (Melcher *et al*. 2015, Glynn *et al*. 2017). They are thus genetically unrelated to either the granitoids of the Dete-Kamativi inlier, or to the early pegmatites. There is no evidence of any parental granite magmatism in the Kamativi area at this time, nor is there clear evidence for localized crustal melting in the local country rocks. The melts that formed the late pegmatites appear to have migrated from depth, before stalling and crystallizing when they reached a depth at which stress conditions were favorable for sill emplacement (Menand 2011). There is very little information available on the tectonic setting of the Kamativi area at this time, although some workers have identified Mesoproterozoic orogenesis in northern Zimbabwe and southern Zambia that is tentatively correlated with the Irumide Belt (Goscombe *et al*. 2000, Karmakar & Schenk 2016). The Kamativi pegmatite may thus correspond to the *ca*. 1050–950 Ma peraluminous, post-tectonic granitoid suite in the Irumide Belt of Zambia, which is considered to have formed by melting of crustal sources (De Waele *et al*. 2006).

Source of the late pegmatite magmas

Classic models of LCT pegmatite formation suggest that they are derived from fertile parental granites. However, the late pegmatites of the Kamativi area (*ca*. 1030 Ma) (Melcher *et al*. 2015, Glynn *et al*. 2017) are around a billion years younger than the adjacent exposed granitoids (2080–2010 Ma) (Glynn *et al*. 2020). It could be suggested that buried granitoids occur at depth and are not exposed, but this model would be difficult to reconcile with the fact that the late pegmatites have very low total REE contents (maximum 14.5 ppm), with flat REE patterns, as is typical for highly peraluminous rare-metal pegmatites (Cullers & Graf 1984). Such very low REE contents are difficult to explain by progressive fractional crystallization of a granitic magma (Simons *et al*. 2016) unless there is very extensive fractionation of REE minerals such as monazite (Bea *et al*. 1994). There is no evidence for such granitoids at depth beneath Kamativi. A possible reason for the very low REE concentrations observed in the late pegmatites is remobilization and concentration of REE in discrete alteration zones (Simmons *et al*. 1987). However, Fuchsloch *et al*. (2018) found that highly altered zones in Nb-Ta-Sn pegmatites in Namibia had some of the lowest REE contents. A similar pattern is seen in altered (*i.e*., albitized) samples from the core of the Kamativi Main Pegmatite, which have much lower

REE contents than less-altered samples from the margins.

Flat REE patterns, with low total REE contents, have been observed in the Mt. Mica pegmatite in Maine, USA (Simmons *et al*. 2016). Here, pegmatite REE patterns are distinct from those of the nearby Sebago granite pluton, but very similar to leucosomes found in the Sebago Migmatite Domain (SMD), which formed by partial melting of the pelitic rocks in the Central Maine Belt. This led Simmons *et al*. (2016) to suggest that partial melting of metapelitic rocks in the SMD may have produced the magma that formed the Mt. Mica pegmatite. Similarly, Fuchsloch *et al*. (2018) found that samples of Nb-Ta-Sn pegmatite from the Cape Cross-Uis pegmatite belt in Namibia have much lower total REE contents than the outcropping granitoids. They also describe very flat REE patterns with missing Eu anomalies. The authors suggest that the differences in REE chemistry between pegmatites and granites cannot simply be explained by fractionation, but instead reflect partial melting of a heterogeneous metasedimentary source.

It is widely accepted that S-type granitic melts, and their associated pegmatites, form from melting of mica-rich metasedimentary rocks (Martin & De Vito 2005, Acosta-Vigil *et al*. 2010, Černý *et al*. 2012a, London & Morgan 2012). Although the micas found in these rocks are known to be important hosts of rare-elements (*e.g*., Rb, Cs, Li, *etc*.), many workers have postulated that evaporites may be an important source of B and Li during the melting of metasedimentary rocks to form pegmatite magmas (Jiang & Palmer 1998, Simmons & Webber 2008, Falster 2011, Bradley 2019). In geological terranes that have seen multiple episodes of metamorphism and deformation, identifying the presence of evaporites may prove challenging. However, metasedimentary rocks that are unusually rich in tourmaline may provide a useful link to past boron enrichment related to evaporites or volcanic activity (Jiang *et al*. 1997).

The spatial link between lithium-bearing pegmatites and boron-rich metasedimentary rocks is well documented (Jiang & Palmer 1998) and adds further weight to the idea that evaporites are an important source of boron in forming pegmatite parental magmas. In the Orange River pegmatite belt in Namaqualand, South Africa, Ballouard *et al*. (2020) suggested that the presence of borosilicate minerals such as tourmaline, kornerupine, and werdingite in metasedimentary rocks of the Bushmanland Group points toward the presence of meta-evaporites. They propose that these boron-rich metasediments might have provided the volatile-rich source required to form the lithium pegmatites, which is consistent with research showing that these boron-rich metasedimentary rocks represented the source of the Erongo granite (Trumbull *et al*. 2008). Similarly, in Ireland, tourmaline-rich schists are common in the country rocks to the Leinster pegmatite belt (Barros *et al*. 2020).

The late pegmatites at Kamativi are of broadly similar age to those of the Orange River pegmatite belt (Ballouard *et al*. 2020). Although the Dete-Kamativi inlier represents a relatively restricted area of outcrop, the metasedimentary rocks of the inlier are considered to correlate with better-exposed lithologies in the Magondi Supergroup. Possible source rocks in the Magondi Supergroup that have the potential to provide the volatiles required for formation of pegmatite parental magmas are: (1) the continental rift basin deposits of the Deweras Group (correlated with the Malaputese and Inyantue formations), which include evaporite sequences (Hahn 2002, Master *et al*. 2010); and (2) the back-arc basin deposits of the Piriwiri Group (correlated with the Kamativi Formation). Interestingly, the volcanic rocks of the Piriwiri Group show evidence of widespread boron and carbonate alteration in the form of secondary tourmaline, dolomite, calcite, and siderite replacing primary feldspar (Munyanyiwa *et al*. 1999). This process of boron-rich alteration has led to the formation of rocks that locally contain up to 30% tourmaline (Mapani *et al*. 1999). Thus, we hypothesize that the source for the late pegmatites at Kamativi may have been melting of local Magondi Supergroup metasedimentary successions, although more work will be needed to prove the details of the link between source and pegmatite.

The drivers for melting at Kamativi are not clear. The age of the Main Kamativi Pegmatite is consistent with the Kibaran-age pegmatites of Central Africa and with those of the Orange River Pegmatite Belt (Melcher *et al*. 2017, Ballouard *et al*. 2020). In these areas there is clear evidence that crustal thickening and metamorphism preceded the formation of the pegmatites, although the geodynamic setting can be debated (Hulsbosch *et al*. 2017). However, there is no recorded evidence for metamorphism and deformation at that time in the rocks of the Magondi Supergroup. During the assembly of the supercontinent of Rodinia in the Mesoproterozoic, the Kamativi area would likely have represented the northern margin of the Kalahari Craton (Jacobs *et al*. 2008). Thus, the late pegmatites at Kamativi may provide evidence for collisional orogenesis along this margin, potentially correlating with the Irumide Belt (De Waele *et al*. 2006).

Internal evolution of the late pegmatite magmas and mineralization paragenesis

The petrography of the Main Kamativi Pegmatite reveals a complex paragenesis. Crystallization of this

pegmatite appears to have begun with the marginal zones, which are the least evolved part of the pegmatite body. In these zones, quartz, feldspar, muscovite, and tourmaline crystallized onto the wall-rock contact. Subsequently, in the core of the pegmatite body, the high contents of lithium in the magmas led to spodumene, with some montebrasite and beryl, crystallizing concurrently with quartz and alkali feldspar. As spodumene is the main lithium mineral formed at this time, crystallization must have occurred in the spodumene stability field. This indicates that pressure-temperature conditions during this part (stage 1) of the paragenesis were approximately 300 to 400 MPa and 500 and 700 °C (London 1990).

As crystallization continued, the concentrations of Li and K, in particular, would have decreased in the residual melt. In contrast, Na, Sn, and Ta would have been concentrated into that residual melt. Eventually, a point was reached at which this more sodic melt began to react with the surrounding pegmatite, being emplaced along zones of weakness to form albite-rich bands and irregular veinlets (stage 2). These bands are also associated with crystallization of cassiterite and columbite-group minerals. The sodic melt in some cases appears to have been injected into the country rock, forming, for example, the aplitic veins in the Gwai River Gorge. The albitization was followed by a period of extensive alteration to a quartz-muscovite greisen assemblage (stage 3), with continued crystallization of cassiterite and CGMs.

Columbite-group minerals in the Main Kamativi Pegmatite are generally characterized by a compositional trend, where the Ta ratio increases with only a small change in the Mn ratio, which indicates that fractionation advanced from ferrocolumbite to ferrotantalite. This type of fractionation trend has been recognized in the pegmatites at Uis, Namibia (Fuchsloch *et al*. 2019), and the Presqueira Pegmatite, NW Spain (Llera *et al*. 2019). This fractionation trend has been shown to be controlled by fluorine activity, *i.e*., a low F activity will result in the crystallization of Fe-rich CGMs, with increasing F activity resulting in the crystallization of Mn-rich endmembers (Černý & Ercit 1985, Černý & Ercit 1989, Spilde & Shearer 1992, Abella *et al*. 1995, Bartels *et al*. 2010, Martins *et al*. 2011).The lack of lepidolite in the Main Kamativi Pegmatite indicates that this is a low-F system. The observed increase in Ta ratio, particularly associated with patchy turbid zonation overprinting earlier oscillatory-zoned columbite crystals, possibly indicates later fluid-induced replacement of early-formed Nb-rich columbite by more a Ta-rich composition. Turbid patchy zonation in CGMs has been interpreted to be the result of re-equilibration of early-formed CGMs with late fluids that could be magmatic (Tindle & Breaks 2000, Van Lichtervelde *et al*. 2008), metamorphic (Černý *et al*. 1989), or exsolved from a melt (Zhang *et al*. 2004, Alfonso & Melgarejo 2008, Ballouard *et al*. 2016). Whether the increasing Ta ratio associated with patchy zonation in CGMs in the Main Kamativi Pegmatite is related to crystallization from a fluid-rich melt (Chevychelov *et al*. 2005) or direct crystallization from a fluid (Zhang *et al*. 2004, Alfonso & Melgarejo 2008) is difficult to say. However, it is clear that fluids played an important role in the formation and replacement of CGMs in the Main Kamativi Pegmatite. In the Presqueira Pegmatite, NW Spain, Llera *et al*. (2019) suggested that the replacement of early-formed Nb-rich CGMs by more Ta-rich compositions occurred by interaction with reactive fluids exsolved from a Na-rich melt during the late stages of crystallization. This model fits with the extensive albitization seen in the Main Kamativi Pegmatite. Therefore, CGMs in the Main Kamativi Pegmatite are interpreted to have crystallized under low-F conditions from ferrocolumbite to ferrotantalite, with the Ta ratio increasing further during the late stages of pegmatite formation as a result of reactive fluids associated with albitization. The data points in Figure 8 that sit in the manganocolumbite field are mostly CGMs in greisenised samples. Rijks & Van der Veen (1972) proposed that concentrations of F, Cl, P, and H_2O in the Main Kamativi Pegmatite might have increased during the greisenisation (*i.e*., muscovite-quartz) stage of formation. Therefore, the trend of increasing Mn ratio in greisenised samples may be related to the slight increase in F in the system during greisenisation, although fluctuations in melt and fluid composition are typical in such systems (Llorens González *et al*. 2017).

Although the classic pressure-temperature diagram by London (1984) to explain the stability relations between eucryptite, spodumene, and petalite is widely accepted, there are potentially a number of possible mechanisms that might explain the formation of co-existing spodumene and petalite, as observed at Kamativi. These include: (1) a decrease in pressure; (2) an increase in temperature; and (3) fluid-mediated replacement of primary spodumene. In the Main Kamativi Pegmatite petalite is typically fine-grained and intergrown with spodumene and quartz, forming thin rims around primary spodumene, or as an infill in fractures cutting across primary spodumene crystals. A similar observation was made by Charoy *et al*. (2001) in Li-pegmatites from the Covas de Barroso district of northern Portugal. They attribute the close association of spodumene and petalite to a drop in confining pressure, which resulted in the precipitation of petalite from a thin film at the spodumene-fluid interface. A

similar drop in pressure, due to post-orogenic decompression, could potentially explain the formation of petalite in the Main Kamativi Pegmatite.

Grubb (1973) noted a similar close association of petalite and spodumene in several Zimbabwean pegmatites, which led him to suggest that a local rise in geotherms may result in the formation of petalite at the expense of spodumene. Similar features have been identified in lithium pegmatites at Vredefort, South Africa, and attributed to heating due to meteorite impact (Rajesh *et al*. 2020). However, in Zimbabwe, there are no recognized events that might have caused heating of the Kamativi pegmatite, with the Umkondo mafic magmatism in the area being somewhat older than the pegmatite at 1110 Ga (de Kock *et al*. 2014).

Similar textures to those observed between petalite, spodumene, and quartz in the Main Kamativi Pegmatite have been seen in the Pusila Pluton, South Tibet. Here, Liu *et al*. (2020) observed two generations of spodumene, primary spodumene and secondary spodumene, with petalite being associated with the latter. They suggested that petalite and secondary spodumene formed by either replacement of primary spodumene in a fluid-rich environment or by direct crystallization from a Li-rich fluid. Liu *et al*. (2020) also showed that secondary spodumene, which they interpret to be hydrothermal, typically has a high-Fe content and therefore a low CL response. Although the textures observed at Kamativi are comparable to those at Pusila, there is a difference in Fe content, with fine-grained spodumene in the Main Kamativi Pegmatite typically having a low Fe content. However, this low Fe content does fit with observations by Filip *et al*. (2006) that secondary spodumene, formed by the isochemical replacement of petalite, generally has a low Fe content.

Overall, the most likely explanation for the growth of petalite after spodumene is related to a reduction in pressure. This is consistent with a model in which melts were generated by decompression melting, following a period of crustal thickening, and were emplaced into a zone undergoing post-tectonic extension. This model would be consistent with *P-T* paths recognized in the Irumide Belt in Zambia (De Waele *et al*. 2006), but much more work remains to be done to understand the correlation of this belt with the rocks of the Magondi Belt.

The fourth, lowest-temperature stage of the Kamativi Main Pegmatite paragenesis is marked by the replacement of feldspar, spodumene, and montebrasite by cookeite, apatite, analcime, and clay minerals. The formation of cookeite ± kaolinite at the expense of spodumene during the final stages of the formation of the Main Kamativi Pegmatite provides evidence of a transition to a lower pressure-temperature regime, but also a change in fluid chemistry. Work by Bobos *et al*. (2007) on Li-bearing pegmatites in northern Portugal showed that the formation of cookeite ± quartz occurs at about 2.4 kbar and 240 °C in response to late-stage deuteric alteration, whereas the formation of cookeite ± kaolinite occurs at 2.2 kbar and 220 °C as a result of increasing acidity during argillic alteration. Both of these assemblages have been observed in the Main Kamativi Pegmatite; however, the association of cookeite and quartz is most prevalent, suggesting that the formation of cookeite in the Main Kamativi Pegmatite largely occurred during stage 3 (*i.e*., greisenisation) of the paragenesis. This stage was also associated with alteration of CGMs to give a patchy zonation.

The paragenesis at Kamativi is similar to that described from other spodumene pegmatites worldwide and reflects the magmatic-hydrothermal transition in the pegmatite. A three-stage paragenesis has been described for albite-spodumene pegmatites in the Leinster region of Ireland (Kaeter *et al*. 2018, Barros *et al*. 2020). Here, a first magmatic stage led to the crystallization of early primary K-feldspar, spodumene, quartz, albite, and muscovite. A subsequent transitional stage was associated with a fluid-rich, sodic residual melt, and was followed by a third hydrothermal stage (Barros *et al*. 2020) which is marked by albitization of the pegmatites associated with the growth of cassiterite and columbite-group minerals. Similar features have been described in several other locations including the tin belt of North Carolina (Swanson 2012), the Uis Belt of Namibia (Fuchsloch *et al*. 2018), and the Orange River Belt of South Africa (Ballouard *et al*. 2020). Notably, in spodumene-bearing pegmatites, zones of albitization and greisenisation are very commonly described, but the shape of the zones as described in the literature appears to vary significantly.

Conclusions

There are two distinct groups of pegmatite in the Kamativi area of Zimbabwe, including (1) early pegmatites that, based on field relationships, are most likely related to the *ca*. 2000 Ma Magondi Orogeny and (2) late pegmatites dated (U-Pb in coltan) at *ca*. 1030 Ma (Melcher *et al*. 2015, Glynn *et al*. 2017). The late pegmatite group includes the Main Kamativi Pegmatite, which has been mined for tin and remains prospective for lithium. The temporal disparity between the late pegmatites (*ca*. 1030 Ma) and the country rock granitoids (*ca*. 2000 Ma) (Melcher *et al*. 2017, Glynn *et al*. 2020) clearly indicates that these granitoids cannot be parental to the late pegmatites. The late pegmatites at Kamativi are thus a good

example of rare-metal pegmatites that have no clear link to a parental granite. We suggest that these pegmatites were formed by partial melting of a metasedimentary source, potentially tourmaline-rich rocks and/or meta-evaporites in the Magondi Supergroup succession. The cause of this melting is not clear, although there is evidence of high-temperature metamorphism at this time in the Irumide Belt of Zambia, suggesting a possible correlation.

Mineralogical and geochemical evidence from the Main Kamativi Pegmatite indicates a four-stage paragenesis, in which a spodumene-bearing magmatic assemblage is replaced in three alteration stages. Stage 2 (albitization) and stage 3 (greisenisation) are important in the formation of Sn and Ta mineralization, while the fourth, lowest-temperature stage is marked by the formation of cookeite and kaolinite. The processes that introduce Sn and Ta may be detrimental to preservation of early crystallizing Li-ore minerals. In the Main Kamativi Pegmatite these alteration stages have largely destroyed spodumene and montebrasite to produce assemblages rich in zeolites, clays, and secondary minerals such as cookeite. These alteration processes have the potential both to decrease the lithium content of a pegmatite, particularly in open systems where lithium can be lost to the country rocks, and to alter the mineralogy, which may affect beneficiation and processing of these ores. Source composition and processes such as fractionation are typically cited as the key controls on the composition of a pegmatite (Sn-rich *versus* Sn-poor). However, the evidence from Kamativi indicates that late-stage alteration processes may also control pegmatite mineralization, and thus understanding the mineral paragenesis of rare-metal pegmatites is essential for exploration targeting.

Acknowledgments

This paper is published with the permission of the Executive Director of the British Geological Survey. The research presented in this paper was supported by the British Geological Survey NC-ODA grant NE/R000069/1: *Geoscience for Sustainable Futures*. This paper is also a contribution to NERC Highlight Topic NE/V006932/1 LiFT (Lithium for Future Technology).

Zimbabwe Lithium, the Zimbabwe Mining Development Corporation, and Premier African Minerals are thanked for providing us with access to their exploration locations.

References

Abella, P.A., Draper, J.-C.M., & Cordomi, M.C. (1995) Nb-Ta-minerals from the Cap de Creus pegmatite field, eastern Pyrenees: Distribution and geochemical trends. *Mineralogy and Petrology* **55**, 53–69.

Acosta-Vigil, A., Buick, I., Hermann, J., Cesare, B., Rubatto, D., London, D., & Morgan, G.B. (2010) Mechanisms of Crustal Anatexis: A Geochemical Study of Partially Melted Metapelitic Enclaves and Host Dacite, SE Spain. *Journal of Petrology* **51**, 785–821.

Alfonso, P. & Melgarejo, J.C. (2008) Fluid evolution in the zoned rare-element pegmatite field at Cap de Creus, Catalonia, Spain. *Canadian Mineralogist* **46**, 597–617.

Ballouard, C., Poujol, M., Boulvais, P., Branquet, Y., Tartèse, R., & Vigneresse, J.-L. (2016) Nb-Ta fractionation in peraluminous granites: A marker of the magmatic-hydrothermal transition. *Geology* **44**, 231–234.

Ballouard, C., Elburg, M.A., Tappe, S., Reinke, C., Ueckermann, H., & Doggart, S. (2020) Magmatic-hydrothermal evolution of rare metal pegmatites from the Mesoproterozoic Orange River pegmatite belt (Namaqualand, South Africa). *Ore Geology Reviews* **116**, 103252.

Barros, R. & Menuge, J. F. (2016) The Origin of Spodumene Pegmatites Associated With the Leinster Granite In Southeast Ireland. *Canadian Mineralogist* **54**, 847–862.

Barros, R., Kaeter, D., Menuge, J.F., & Škoda, R. (2020) Controls on chemical evolution and rare element enrichment in crystallising albite-spodumene pegmatite and wallrocks: Constraints from mineral chemistry. *Lithos* 352–353, 105289.

Bartels, A., Holtz, F., & Linnen, R.L. (2010) Solubility of manganotantalite and manganocolumbite in pegmatitic melts. *American Mineralogist* **95**, 537–544.

Bea, F., Pereira, M.D., Corretgé, L.G., & Fershtater, G.B. (1994) Differentiation of strongly peraluminous, perphosphorus granites: The pedrobernardo pluton, central Spain. *Geochimica et Cosmochimica Acta* **58**, 2609–2627.

Bobos, I., Vieillard, P., Charoy, B., & Noronha, F. (2007) Alteration of spodumene to cookeite and its pressure and temperature stability conditions in Li-bearing aplite-pegmatites from northern Portugal. *Clays and Clay Minerals* **55**, 295–310.

Bradley, D.C. (2019) Tectonic and paleoclimatic controls of lithium-cesium-tantalum (LCT) pegmatite genesis, exhumation, and preservation in the Appalachians. *Canadian Mineralogist* **57**, 715–717.

Bradley, D.C., McCauley, A.D., & Stillings, L.L. (2017) *Mineral-deposit model for lithium-cesium-tantalum pegmatites*. United States Geological Survey, Report Number 2010-5070-O. United States Geological Survey, United States of America.

Cameron, E.N., Jahns, R.H., McNair, A.H., & Page, L.R. (1949) *Internal Structure of Granitic Pegmatites, volume 2*. Society of Economic Geologists, Littleton, Colorado, United Sates of America.

Černý, P. (1992) Geochemical and petrogenetic features of mineralization in rare-element granitic pegmatites in the light of current research. *Applied Geochemistry* **7**, 393–416.

Černý, P. & Ercit, T.S. (1985) Some recent advances in the mineralogy and geochemistry of Nb and Ta in rare-element granitic pegmatites. *Bulletin de Minéralogie* **108**, 499–532.

Černý, P. & Ercit, T.S. (1989) Mineralogy of Niobium and Tantalum: Crystal Chemical Relationships, Paragenetic Aspects and Their Economic Implications. *In* Lanthanides, Tantalum and Niobium (P. Möller, P. Černý, & F. Saupé, eds.). Springer Berlin Heidelberg, Berlin, Heidelberg, Germany (27–79).

Černý, P. & Ercit, T.S. (2005) The Classification of granitic pegmatites revisited. *Canadian Mineralogist* **43**, 2005–2026.

Černý, P., Chapman, R., Chackowsky, L., & Ercit, T. (1989) A ferrotantalite-ferrotapiolite intergrowth from Spittal ad Drau, Carinthia, Austria. *Mineralogy and Petrology* **41**, 53–63.

Černý, P., London, D., & Novák, M. (2012a) Granitic Pegmatites as Reflections of Their Sources. *Elements* **8**, 289–294.

Černý, P., Teertstra, D.K., Chapman, R., Selway, J.B., Hawthorne, F.C., Ferreira, K., Chackowsky, L.E., Wang, X.-J., & Meintzer, R.E. (2012b) Extreme fractionation and deformation of the leucogranite – pegmatite suite at Red Cross Lake, Manitoba, Canada. IV. Mineralogy. *Canadian Mineralogist* **50**, 1839–1875.

Charoy, B., Noronha, F., & Lima, A. (2001) Spodumene – petalite – eucryptite: Mutual relationships and pattern of alteration in Li-rich aplite–pegmatite dykes from northern Portugal. *Canadian Mineralogist* **39**, 729–746.

Chevychelov, V.Y., Zaraisky, G., Borisovskii, S., & Borkov, D. (2005) Effect of melt composition and temperature on the partitioning of Ta, Nb, Mn, and F between granitic (alkaline) melt and fluorine-bearing aqueous fluid: Fractionation of Ta and Nb and conditions of ore formation in rare-metal granites. *Petrology* **13**, 305–321.

Cronwright, M.S. & Derbyshire, J. (2018) *NI 43-101 Technical Report*. Chimata Gold Corporation Kamativi Lithium Tailings Project, Matabeleland North Province, Zimbabwe.

Cullers, R.L. & Graf, J.L. (1984) Rare earth elements in igneous rocks of the continental crust: Intermediate and silicic rocks–ore petrogenesis. *Developments in Geochemistry* **2**, 275–316.

Dai, H., Wang, D., Liu, L., Yu, Y., & Dai, J. (2019) Geochronology and Geochemistry of Li(Be)-Bearing Granitic Pegmatites from the Jiajika Superlarge Li-Polymetallic Deposit in Western Sichuan, China. *Journal of Earth Science* **30**, 707–727.

de Kock, M.O., Ernst, R., Söderlund, U., Jourdan, F., Hofmann, A., Le Gall, B., Bertrand, H., Chisonga, B.C., Beukes, N., Rajesh, H.M., Moseki, L.M., & Fuchs, R. (2014) Dykes of the 1.11Ga Umkondo LIP, Southern Africa: Clues to a complex plumbing system. *Precambrian Research* **249**, 129–143.

De Waele, B., Wingate, M.T.D., Fitzsimons, I.C.W., & Mapani, B.S.E. (2003) Untying the Kibaran knot: A reassessment of Mesoproterozoic correlations in southern Africa based on SHRIMP U-Pb data from the Irumide belt. *Geology* **31**, 509–512.

De Waele, B., Kampunzu, A.B., Mapani, B.S.E., & Tembo, F. (2006) The Mesoproterozoic Irumide belt of Zambia. *Journal of African Earth Sciences* **46**, 36–70.

Dittrich, T., Seifert, T., Schulz, B., Hagemann, S., Gerdes, A., & Pfänder, J. (2019) Geological Settings of Archean Rare-Metal Pegmatites. *In* Archean Rare-Metal Pegmatites in Zimbabwe and Western Australia: Geology and Metallogeny of Pollucite Mineralisations (T. Dittrich, T. Seifert, B. Schulz, S. Hagemann, A. Gerdes, & J. Pfänder, eds.). Springer International Publishing (23–59).

Falster, A.U., Simmons, W.B., & Webber, K.L. (2011) Origin of the Hoskin Lake Pegmatites, Florence Co., Wisconsin. Geological Society of America 45th Annual meeting Abstracts with Programs **43**, 43.

Filip, J., Novák, M., Beran, A., & Zbořil, R. (2006) Crystal chemistry and OH defect concentrations in spodumene from different granitic pegmatites. *Physics and Chemistry of Minerals* **32**, 733–746.

Fuchsloch, W.C., Nex, P.A.M., & Kinnaird, J.A. (2018) Classification, mineralogical and geochemical variations in pegmatites of the Cape Cross-Uis pegmatite belt, Namibia. *Lithos* **296–299**, 79–95.

Fuchsloch, W.C., Nex, P.A.M., & Kinnaird, J.A. (2019) The geochemical evolution of Nb–Ta–Sn oxides from pegmatites of the Cape Cross–Uis pegmatite belt, Namibia. *Mineralogical Magazine* **83**, 161–179.

Garate-Olave, I., Roda-Robles, E., Gil-Crespo, P.P., Pesquera, A., & Errandonea-Martin, J. (2020) The Tres Arroyos Granitic Aplite-Pegmatite Field (Central Iberian Zone, Spain): Petrogenetic Constraints from Evolution of Nb-Ta-Sn Oxides, Whole-Rock Geochemistry and U-Pb Geochronology. *Minerals* **10**, 1008.

Glynn, S.M. (2017) *Geochronology and Evolution of the Magondi Belt*. University of the Witwatersrand, Johannesburg, South Africa.

Glynn, S.M., Master, S., Wiedenbeck, M., Davis, D.W., Kramers, J.D., Belyanin, G.A., Frei, D., & Oberthür, T. (2017) The Proterozoic Choma-Kalomo Block, SE Zambia: Exotic terrane or a reworked segment of the Zimbabwe Craton? *Precambrian Research* **298**, 421–438.

Glynn, S.M., Master, S., Frei, D., & Wiedenbeck, M. (2020) U-Pb zircon geochronology of the Dete-Kamativi Inlier, NW Zimbabwe, with implications for the western margin

of the Archaean Zimbabwe Craton. *Precambrian Research* **346**, 105824.

Goodenough, K.M., Lusty, P.A.J., Roberts, N.M.W., Key, R.M., & Garba, A. (2014) Post-collisional Pan-African granitoids and rare metal pegmatites in western Nigeria: Age, petrogenesis, and the 'pegmatite conundrum'. *Lithos* **200–201**, 22–34.

Goscombe, B., Armstrong, R., & Barton, J.M. (2000) Geology of the Chewore Inliers, Zimbabwe: Constraining the Mesoproterozoic to Palæozoic evolution of the Zambezi Belt. *Journal of African Earth Sciences* **30**, 589–627.

Grubb, P. (1973) Paragenesis of spodumene and other lithium minerals in some Rhodesian pegmatites. *In* Symposium on Granites, Gneisses and Related Rocks. Geological Society of South Africa **3**, 201–216.

Hahn, L. (2002) On the Stratigraphy of the Palaeoproterozoic Deweras and Lomagundi Groups (Magondi Supergroup) in Zimbabwe. *South African Journal of Geology* **105**, 193–204.

Hargrove, U.S., Hanson, R.E., Martin, M.W., Blenkinsop, T.G., Bowring, S.A., Walker, N., & Munyanyiwa, H. (2003) Tectonic evolution of the Zambezi orogenic belt: Geochronological, structural, and petrological constraints from northern Zimbabwe. *Precambrian Research* **123**, 159–186.

Holzer, L., Frei, R., Barton, J.M., & Kramers, J.D. (1998) Unraveling the record of successive high grade events in the Central Zone of the Limpopo Belt using Pb single phase dating of metamorphic minerals. *Precambrian Research* **87**, 87–115.

Horstwood, M.S.A., Nesbitt, R.W., Noble, S.R., & Wilson, J.F. (1999) U-Pb zircon evidence for an extensive early Archean craton in Zimbabwe: A reassessment of the timing of craton formation, stabilization, and growth. *Geology* **27**, 707–710.

Hulsbosch, N., Van Daele, J., Reinders, N., Dewaele, S., Jacques, D., & Muchez, P. (2017) Structural control on the emplacement of contemporaneous Sn-Ta-Nb mineralized LCT pegmatites and Sn bearing quartz veins: Insights from the Musha and Ntunga deposits of the Karagwe-Ankole Belt, Rwanda. *Journal of African Earth Sciences* **134**, 24–32.

Jacobs, J., Pisarevsky, S., Thomas, R.J., & Becker, T. (2008) The Kalahari Craton during the assembly and dispersal of Rodinia. *Precambrian Research* **160**, 142–158.

Jelsma, H.A., Vinyu, M.L., Wijbrans, J.R., Verdurmen, E., Valbracht, P., & Davies, G. (1996) Constraints on Archaean crustal evolution of the Zimbabwe craton: A U-Pb zircon, Sm-Nd and Pb-Pb whole-rock isotope study. *Contributions to Mineralogy and Petrology* **124**, 55–70.

Jelsma, H.A. & Dirks, P.H.G.M. (2002) Neoarchaean tectonic evolution of the Zimbabwe Craton. *Geological Society, London, Special Publications* **199**, 183–211.

Jiang, S.-Y. & Palmer, M.R. (1998) Boron isotope systematics of tourmaline from granites and pegmatites; a synthesis. *European Journal of Mineralogy* **10**, 1253–1265.

Jiang, S.-Y., Palmer, M., Peng, Q.-M., & Yang, J.-H. (1997) Chemical and stable isotopic compositions of Proterozoic metamorphosed evaporites and associated tourmalines from the Houxianyu borate deposit, eastern Liaoning, China. *Chemical Geology* **135**, 189–211.

Johnson, S.P., Rivers, T., & De Waele, B. (2005) A review of the Mesoproterozoic to early Palaeozoic magmatic and tectonothermal history of south–central Africa: Implications for Rodinia and Gondwana. *Journal of the Geological Society* **162**, 433–450.

Kaeter, D., Barros, R., Menuge, J.F., & Chew, D.M. (2018) The magmatic–hydrothermal transition in rare-element pegmatites from southeast Ireland: LA-ICP-MS chemical mapping of muscovite and columbite–tantalite. *Geochimica et Cosmochimica Acta* **240**, 98–130.

Karmakar, S. & Schenk, V. (2016) Mesoproterozoic UHT metamorphism in the Southern Irumide Belt, Chipata, Zambia: Petrology and in situ monazite dating. *Precambrian Research* **275**, 332–356.

Kinnaird, J.A., Nex, P.A., & Milani, L. (2016) Tin in Africa. *Episodes* **39**, 361–380.

Liu, C., Wang, R.-C., Wu, F.-Y., Xie, L., Liu, X.-C., Li, X.-K., Yang, L., & Li, X.-J. (2020) Spodumene pegmatites from the Pusila pluton in the higher Himalaya, South Tibet: Lithium mineralization in a highly fractionated leucogranite batholith. *Lithos* **358–359**, 105421.

Llera, A.R., Fuertes-Fuente, M., Cepedal, A., & Martin-Izard, A. (2019) Barren and Li–Sn–Ta Mineralized Pegmatites from NW Spain (Central Galicia): A Comparative Study of Their Mineralogy, Geochemistry, and Wallrock Metasomatism. *Minerals* **9**, 739.

Llorens González, T., García Polonio, F., López Moro, F.J., Fernández Fernández, A., Sanz Contreras, J.L., & Moro Benito, M.C. (2017) Tin-tantalum-niobium mineralization in the Penouta deposit (NW Spain): Textural features and mineral chemistry to unravel the genesis and evolution of cassiterite and columbite group minerals in a peraluminous system. *Ore Geology Reviews* **81**, 79–95.

Lockett, N.H. (1979) *The geology of the county around Dett*. Rhodesia Geological Survey, Salisbury.

London, D. (1984) Experimental phase equilibria in the system $LiAlSiO_4$–SiO_2–H_2O: A petrogenetic grid for lithiumx-rich pegmatites. *American Mineralogist* **69**, 995–1004.

London, D. (1990) Internal differentiation of rare-element pegmatites: A synthesis of recent research. *Geological Society of America Special Paper* **246**, 35–50.

London, D. (2005) Granitic pegmatites: An assessment of current concepts and directions for the future. *Lithos* **80**, 281–303.

London, D. (2014) A petrologic assessment of internal zonation in granitic pegmatites. *Lithos* **184–187**, 74–104.

London, D. (2018) Ore-forming processes within granitic pegmatites. *Ore Geology Reviews* **101**, 349–383.

London, D. & Morgan, G.B. (2012) The Pegmatite Puzzle. *Elements* **8**, 263–268.

Mapani, B., Munyanyiwa, H., & Manyanhaire, M. (1999) Significance of a large tourmaline province in the Piriwiri Group rocks, Magondi belt, northeastern Zimbabwe. *Journal of African Earth Sciences* **28**, 46–46.

Markwitz, V., Maier, W.D., González-Álvarez, I., McCuaig, T.C., & Porwal, A. (2010) Magmatic nickel sulfide mineralization in Zimbabwe: Review of deposits and development of exploration criteria for prospectivity analysis. *Ore Geology Reviews* **38**, 139–155.

Martin, R.F. & De Vito, C. (2005) The Patterns of Enrichment in Felsic Pegmatites Ultimately Depend on Tectonic Setting. *Canadian Mineralogist* **43**, 2027–2048.

Martins, T., Lima, A., Simmons, W.B., Falster, A.U., & Noronha, F. (2011) Geochemical Fractionation of Nb–Ta Oxides in Li-bearing Pegmatites from The Barroso–Alvão Pegmatite Field, Northern Portugal. *Canadian Mineralogist* **49**, 777–791.

Martins, T., Roda-Robles, E., Lima, A., & de Parseval, P. (2012) Geochemistry and Evolution of Micas in The Barroso–Alvão Pegmatite Field, Northern Portugal. *Canadian Mineralogist* **50**, 1117–1129.

Master, S., Bekker, A., & Hofmann, A. (2010) A review of the stratigraphy and geological setting of the Palaeoproterozoic Magondi Supergroup, Zimbabwe – Type locality for the Lomagundi carbon isotope excursion. *Precambrian Research* **182**, 254–273.

McDonough, W.F. & Sun, S.S. (1995) The composition of the Earth. *Chemical Geology* **120**, 223–253.

Melcher, F., Graupner, T., Gäbler, H.-E., Sitnikova, M., Henjes-Kunst, F., Oberthür, T., Gerdes, A., & Dewaele, S. (2015) Tantalum–(niobium–tin) mineralisation in African pegmatites and rare metal granites: Constraints from Ta–Nb oxide mineralogy, geochemistry and U–Pb geochronology. *Ore Geology Reviews* **64**, 667–719.

Melcher, F., Graupner, T., Gäbler, H.-E., Sitnikova, M., Oberthür, T., Gerdes, A., Badanina, E., & Chudy, T. (2017) Mineralogical and chemical evolution of tantalum–(niobium–tin) mineralisation in pegmatites and granites. Part 2: Worldwide examples (excluding Africa) and an overview of global metallogenetic patterns. *Ore Geology Reviews* **89**, 946–987.

Menand, T. (2011) Physical controls and depth of emplacement of igneous bodies: A review. *Tectonophysics* **500**, 11–19.

Mineralogical Association of Canada (2019) *The Canadian Mineralogist List of Symbols for Rock- and Ore-Forming Minerals*. Mineralogical Association of Canada, Canada. Available from <https://www.mineralogicalassociation.ca/wordpress/wp-content/uploads/2020/01/symbols.pdf>.

Müller, A., Romer, R.L., & Pedersen, R.-B. (2017) The Sveconorwegian Pegmatite Province – Thousands of Pegmatites Without Parental Granites. *Canadian Mineralogist* **55**, 283–315.

Munyanyiwa, H., Manyanhaire, M., Mapani, B., Dube, J., & Nyarufuro, B. (1999) Geochemistry of felsic volcanics in the Magondi basin (northwestern Zimbabwe): Evidence for regional carbonate and boron alteration. *Journal of African Earth Sciences* **28**, 56.

Norton, J.J. (1983) Sequence of mineral assemblages in differentiated granitic pegmatites. *Economic Geology* **78**, 854–874.

Oberthür, T., Davis, D.W., Blenkinsop, T.G., & Höhndorf, A. (2002) Precise U–Pb mineral ages, Rb–Sr and Sm–Nd systematics for the Great Dyke, Zimbabwe—constraints on late Archean events in the Zimbabwe craton and Limpopo belt. *Precambrian Research* **113**, 293–305.

Pehlken, A., Albach, S., & Vogt, T. (2017) Is there a resource constraint related to lithium ion batteries in cars? *The International Journal of Life Cycle Assessment* **22**, 40–53.

Rajesh, H.M., Knoper, M.W., Belyanin, G.A., Safonov, O.G., & Schmidt, C. (2020) Petalite postdating spodumene in pegmatite as a consequence of the ~2.02 Ga meteorite impact in the Vredefort structure, southern Africa. *Lithos* **376–377**, 105760.

Rijks, H.R.P. & van der Veen, A.H. (1972) The Geology of the Tin-Bearing Pegmatites in the Eastern Part of the Kamativi District, Rhodesia. *Mineralium Deposita* **7**, 383–395.

Roda-Robles, E., Pesquera, A., Gil-Crespo, P.P., Vieira, R., Lima, A., Garate-Olave, I., Martins, T., & Torres-Ruiz, J. (2016) Geology and mineralogy of Li mineralization in the Central Iberian Zone (Spain and Portugal). *Mineralogical Magazine* **80**, 103–126.

Roda-Robles, E., Villaseca, C., Pesquera, A., Gil-Crespo, P.P., Vieira, R., Lima, A., & Garate-Olave, I. (2018) Petrogenetic relationships between Variscan granitoids and Li-(F-P)-rich aplite-pegmatites in the Central Iberian Zone: Geological and geochemical constraints and implications for other regions from the European Variscides. *Ore Geology Reviews* **95**, 408–430.

Rollinson, H.R. & Whitehouse, M. (2011) The growth of the Zimbabwe Craton during the late Archaean: An ion microprobe U–Pb zircon study. *Journal of the Geological Society* **168**, 941–952.

Rudnick, R. & Gao, S. (2003) Composition of the continental crust. *In* Treatise On Geochmistry Volume 3 (H.D. Holland & K.K. Turekian, eds.). Elselvier, Amsterdam, Netherlands (1–64).

Sawada, H., Mugandani, E.T., Sato, T., Sawaki, Y., Sakata, S., Isozaki, Y., & Maruyama, S. (2019) Age constraints on the Palaeoproterozoic Lomagundi–Jatuli Event in Zimbabwe: Zircon geochronology of the Magondi Supergroup. *Terra Nova* **31**, 438–444.

Shaw, R.A., Goodenough, K.M., Roberts, N.M.W., Horstwood, M.S.A., Chenery, S.R., & Gunn, A.G. (2016) Petrogenesis of rare-metal pegmatites in high-grade metamorphic terranes: A case study from the Lewisian Gneiss Complex of north-west Scotland. *Precambrian Research* **281**, 338–362.

Shaw, R.A., Goodenough, K.M., Deady, E.A., & Nex, P. (2019) The Kamativi pegmatite: An opportunity for economic development in Zimbabwe? *Canadian Mineralogist* **57**, 791–793.

Simmons, W.B. & Webber, K.L. (2008) Pegmatite genesis: State of the art. *European Journal of Mineralogy* **20**, 421–438.

Simmons, W.B., Lee, M.T., & Brewster, R.H. (1987) Geochemistry and evolution of the South Platte granite-pegmatite system, Jefferson County, Colorado. *Geochimica et Cosmochimica Acta* **51**, 455–471.

Simmons, W.B., Falster, A., Webber, K., Roda-Robles, E., Boudreaux, A.P., Grassi, L.R., & Freeman, G. (2016) Bulk composition of Mt. Mica Pegmatite, Maine, USA: Implications for the origin of an LCT-type pegmatite by anatexis. *Canadian Mineralogist* **54**, 1053–1070.

Simmons, W.B., Falster, A.U., & Freeman, G. (2020) The Plumbago North pegmatite, Maine, USA: A new potential lithium resource. *Mineralium Deposita* **55**, 1505–1510.

Simons, B., Shail, R.K., & Andersen, J.C.Ø. (2016) The petrogenesis of the Early Permian Variscan granites of the Cornubian Batholith: Lower plate post-collisional peraluminous magmatism in the Rhenohercynian Zone of SW England. *Lithos* **260**, 76–94.

Spilde, M.N. & Shearer, C.K. (1992) A comparison of tantalum-niobium oxide assemblages in two mineralogically distinct rare-element granitic pegmatites, Black Hills, South Dakota. *Canadian Mineralogist* **30**, 719–737.

Stewart, D.B. (1978) Petrogenesis of lithium-rich pegmatites. *American Mineralogist* **63**, 970–980.

Swanson, S.E. (2012) Mineralogy of Spodumene Pegmatites and Related Rocks in the Tin–Spodumene Belt of North Carolina and South Carolina, USA. *Canadian Mineralogist* **50**, 1589–1608.

Sweetapple, M.T., Grigson, M.W., Tornatora, P., & Urgine, S. (2019) The Archean Mt. Cattlin spodumene pegmatite group and 3D geochemical mapping of large "unzoned" pegmatites of economic significance. *Canadian Mineralogist* **57**, 803–805.

Tack, L., Wingate, M.T.D., De Waele, B., Meert, J., Belousova, E., Griffin, B., Tahon, A., & Fernandez-Alonso, M. (2010) The 1375Ma "Kibaran event" in Central Africa: Prominent emplacement of bimodal magmatism under extensional regime. *Precambrian Research* **180**, 63–84.

Tindle, A.G. & Breaks, F.W. (2000) Columbite-tantalite mineral chemistry from rare-element granitic pegmatites: Separation Lake area, N.W. Ontario, Canada. *Mineralogy and Petrology* **70**, 165–198.

Trumbull, R., Krienitz, M.-S., Gottesmann, B., & Wiedenbeck, M. (2008) Chemical and boron-isotope variations in tourmalines from an S-type granite and its source rocks: The Erongo granite and tourmalinites in the Damara Belt, Namibia. *Contributions to Mineralogy and Petrology* **155**, 1–18.

USGS (2018) *Lithium Mineral Commodity Summary*. United States Geological Survey, United States of America.

Van Lichtervelde, M., Grégoire, M., Linnen, R., Béziat, D., & Salvi, S. (2008) Trace element geochemistry by laser ablation ICP-MS of micas associated with Ta mineralization in the Tanco pegmatite, Manitoba, Canada. *Contributions to Mineralogy and Petrology* **155**, 791–806.

Villaros, A. & Pichavant, M. (2019) Mica-liquid trace elements partitioning and the granite-pegmatite connection: The St-Sylvestre complex (Western French Massif Central). *Chemical Geology* **528**, 119265.

Von Knorring, O. & Condliffe, E. (1987) Mineralized pegmatites in Africa. *Geological Journal* **22**, 253–270.

Wilde, A., Otto, A., & McCracken, S. (2021) Geology of the Goulamina spodumene pegmatite field, Mali. *Ore Geology Reviews* **134**, 104162.

Zhang, A., Wang, R., Hu, H., Zhang, H., Zhu, J., & Chen, X. (2004) Chemical evolution of Nb-Ta oxides and zircon from the Koktokay No. 3 granitic pegmatite, Altai, northwestern China. *Mineralogical Magazine* **68**, 739–756.

Zhang, X., Zhang, H., Ma, Z.-L., Tang, Y., Lv, Z.-H., Zhao, J.-Y., & Liu, Y.-L. (2016) A new model for the granite–pegmatite genetic relationships in the Kaluan–Azubai–Qiongkuer pegmatite-related ore fields, the Chinese Altay. *Journal of Asian Earth Sciences* **124**, 139–155.

Zimbabwe Lithium (2020) *Kamativi Tailings Project*. Available from: <www.zimlithium.com>.

Received March 12, 2021. Revised manuscript accepted September 7, 2021.

This manuscript was handled by Guest Editor Tania Martins and Editor Lee Groat.